On the influence of steam on the CO2 chemisorption capacity of a hydrotalcite-based adsorbent for SEWGS applications

Chemical Engineering Journal 314 (2017) 554–569

Contents lists available at ScienceDirect

Chemical Engineering Journal

journal homepage: www.elsevier.com/locate/cej

On the influence of steam on the CO_2 chemisorption capacity of a hydrotalcite-based adsorbent for SEWGS applications

Kai Coenen [a], Fausto Gallucci [a,*], Gianmaria Pio [a], Paul Cobden [b], Eric van Dijk [b], Emiel Hensen [a], Martin van Sint Annaland [a]

[a] Department of Chemical Engineering and Chemistry, Eindhoven University of Technology, P.O. Box 513, Eindhoven, The Netherlands
[b] Sustainable Process Technology, ECN, P.O. Box 1, 1755ZG Petten, The Netherlands

HIGHLIGHTS

- At least four different adsorption sites participate in the sorption/desorption of CO_2 and H_2O on hydrotalcites.
- Regeneration with steam leads to a significant increase in the CO_2 cyclic working capacity of the sorbent.
- A mechanism is proposed that describes multiple experiments in TGA and packed beds.

GRAPHICAL ABSTRACT

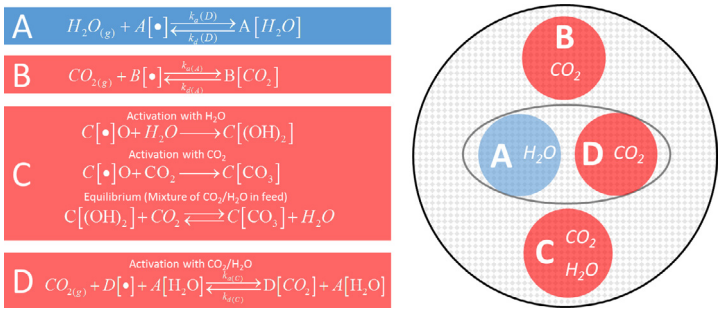

ARTICLE INFO

Article history:
Received 1 November 2016
Received in revised form 1 December 2016
Accepted 2 December 2016
Available online 5 December 2016

Keywords:
Cyclic working capacity
Effect of steam on sorption capacity
Hydrotalcite
CO_2 capture

ABSTRACT

Hydrotalcite-based adsorbents have shown great potential for use in sorption-enhanced water-gas-shift applications. A combination of thermogravimetric experiments and breakthrough experiments have been carried out to elucidate the effect of steam on the CO_2 cyclic sorption capacity on a K-promoted hydrotalcite-based adsorbent. Different TGA cycles have been designed to study the mass change on sorbents exposed to different sequences of different CO_2/H_2O/N_2 mixtures. Because the complex sorption/desorption and replacement phenomena cannot be explained by TGA experiments only, additional information from breakthrough experiments in a packed bed reactor was used to correlate the observed total mass change in the TGA cycles to the phenomena prevailing on the sorbent.

A mechanism has been developed which is able to describe the cyclic working capacity, for both CO_2 and H_2O under different experimental conditions. It was found that at least four different adsorption sites participate in the sorption/desorption of CO_2 and H_2O. Two adsorption sites can be regenerated with N_2, whereas the other adsorption sites require the presence of H_2O or CO_2 to be desorbed. Regeneration of the adsorbent with steam leads to a significant increase in the CO_2 cyclic working capacity from 0.3 to 0.53 mmol/g compared to a dry regeneration with N_2 using the same cycle times.

1. Introduction

Increasing concerns about the effects of the increase in the CO_2 levels in the earth's atmosphere related to the combustion of fossil resources on climate change has put the mitigation of anthropogenic CO_2 emissions high on the agenda of policy makers [1].

* Corresponding author.
E-mail address: F.Gallucci@tue.nl (F. Gallucci).

http://dx.doi.org/10.1016/j.cej.2016.12.013
1385-8947/

Nomenclature

A	cyclic working capacity of a adsorption site for H_2O
B	cyclic working capacity of a adsorption site for CO_2
BET	Brunauer-Emmett-Teller method for surface area determination
C	cyclic working capacity of a adsorption site for CO_2
C_{eq}	cyclic working capacity (mass change) if H_2O is replaced with CO_2 on site C (for a feed of both CO_2 and H_2O)
CV	check valve
CWC	cyclic working capacity
D	cyclic working capacity of a adsorption site for CO_2
FH	needle valve with indicator
FC	mass flow controller
FS	volume flow measurement
PI	pressure indicator
PBR	packed bed reactor
PC	back pressure regulator
PCO_2	partial pressure of CO_2 [bar]
PH_2O	partial pressure of H_2O [bar]
QA	gas detection system
SV	automatic valve
TC	temperature controller
TE	temperature indicator
TGA	thermo-gravimetric analysis
WT	symbol for balance
XRD	X-ray crystallography

Carbon Capture and Storage (CCS) is one strategy to reduce CO_2 emissions from fossil fuel based power plants and other energy intensive industries, which entails capture of the CO_2 from process streams (pre-combustion or post-combustion) with subsequent storage in depleted gas and oil fields. However, high investment and operational costs associated with in particular the CO_2 capture step lead to increased costs of electricity, effectively hampering further exploitation of CCS technologies [2].

Sorption-enhanced water-gas-shift (SEWGS) is a promising concept for pre-combustion CO_2 capture, which combines the water-gas-shift (WGS) reaction with CO_2 removal in a single unit operation. Its main advantages are high CO conversion rates attainable at high temperatures (400 °C), which is due to the shift of the WGS equilibrium, and a lower steam to CO_2 ratio leading to reduced operational costs in comparison to alternative processes, such as the conventional Selexol process [3,4]. It has been demonstrated that SEWGS can reduce the CO_2 capture costs by more than 17% compared to Selexol in an integrated gasification combined cycle (IGCC) power plant [5]. The SEWGS process is based on reversible in situ CO_2 adsorption on solid materials at temperatures between 350 and 550 °C [6]. Multiple columns are used in parallel to deal with the periodic behavior of the adsorption/desorption cycles and obtain a continuous process.

Hydrotalcite-based adsorbents are interesting candidates for SEWEGS applications because of their high stability [7,8], fast adsorption/desorption kinetics [9,10] and high selectivity for CO_2 compared to CO and H_2. Hydrotalcites belong to the group of anionic clays and can be chemically described by the formula $[Mg^{2+}_{1x}\text{-}Al^{3+}(OH)_2]^{x+}\ (A^{n-})_{x/n} * mH_2O$, where A is the interlayer anion [11]. The most common stoichiometry for hydrotalcites is the double magnesium-aluminum hydroxide with formula $Mg_6Al_2(HO)_{16}CO_3^{2-x}$ 4 H_2O. The molar ratio of Mg/Al can vary between 1.7 and 4 [12]. Small Mg/Al ratios can lead to segregation of $Al(OH)_3$, while high Mg/Al ratios cause the formation of a separate $Mg(OH)_2$ phase [13]. At higher Mg/Al ratios the basicity increases, which can be beneficial for the absorption of sour gases such as CO_2 [11]. The basicity can be further improved by promotion with alkaline anions [8]. It has been frequently reported in the literature that promotion of hydrotalcites with K_2CO_3 can increase the sorption capacity of CO_2 [14,15,10]. At higher Mg/Al ratios, also $MgCO_3$ may form at high partial pressures of steam and CO_2, which can lead to mechanical stability issues [8,16]. A further aspect is that the initial layered structure of the anionic clay present at room temperatures disappears when the material is heated to elevated temperatures. During the heating process the original structure changes to a $Mg(Al)O_x$ mixed metal oxide releasing CO_2 and H_2O [11,17]. Typical calcination temperatures in air are between 673 and 773 K. Hydrotalcites have a memory effect as reconstruction to the layered structure is observed by exposing the material to water [18]. Different K_2CO_3 promoted and unpromoted hydrotalcites produced by SASOL (Germany) have been used in various studies, as they are available in large quantities and in different chemical compositions which can be used in different applications [19–26].

A SEWGS cycle usually consists of about five main steps. After saturation of the sorbent, a rinse step is used to improve the CO_2 purity by preventing slip of H_2 into the CO_2 stream [21]. The depressurization of the column is followed by a purge with steam to increase the recovery of CO_2, thereby also increasing the cyclic CO_2 capacity of the adsorbent [21]. Although it has been reported in the literature that steam can increase the CO_2 adsorption capacity of potassium-promoted hydrotalcites, the mechanisms of H_2O and CO_2 adsorption/desorption on this material are not yet fully understood [8,10,23,26]. It has been shown in an earlier publication that a K_2CO_3 promoted hydrotalcite (Mg/Al-ratio = 0.54) has a very high adsorption capacity for steam, but the aspect of water adsorption has been largely neglected in the literature [27]. However, for detailed reactor modeling and process evaluation, these effects are very important, because they have an effect on the hydrodynamics (change in superficial gas velocity) and the adsorption behavior of the hydrotalcite [24]. Therefore, the objective of this work is to improve the understanding of the effect of steam on the cyclic sorption capacity of a hydrotalcite-based adsorbent by elucidating the complex behavior of the adsorption/desorption phenomena of CO_2 and H_2O, using thermogravimetric analyses (TGA) and breakthrough experiments in a packed bed reactor. On the basis of the obtained experimental data, a model is formulated involving different sites on the absorbent that can describe the cyclic working capacity of CO_2 and H_2O at different operating conditions.

2. Materials and methods

A potassium-promoted hydrotalcite-based adsorbent with a Mg/Al ratio of 0.54 and a potassium loading of approximately 20 wt% in pellet form (4.7 × 4.7 mm), produced by Sasol Germany, was used in the experiments and will be further denoted as KMG30. The material was milled to powder and characterized using a helium pycnometer (Quantachrome Upyc 1200e), BET (Thermo Fischer Surfer), Mercury porosimetry (Thermo Fischer Pascal 140/440), XRD (Rigaku Miniflex 600) and SEM-EDX to study the morphology. Characterization results have been already published elsewhere [27]. The surface area determined by the BET method is about 112 m^2/g. XRD has shown, that KMG30 is highly amorphous material under the measured conditions. Periclase (MgO) and spinel ($Mg_{0.4}Al_{2.4}O_4$) were identified according to the peak positions from the ICCD database.

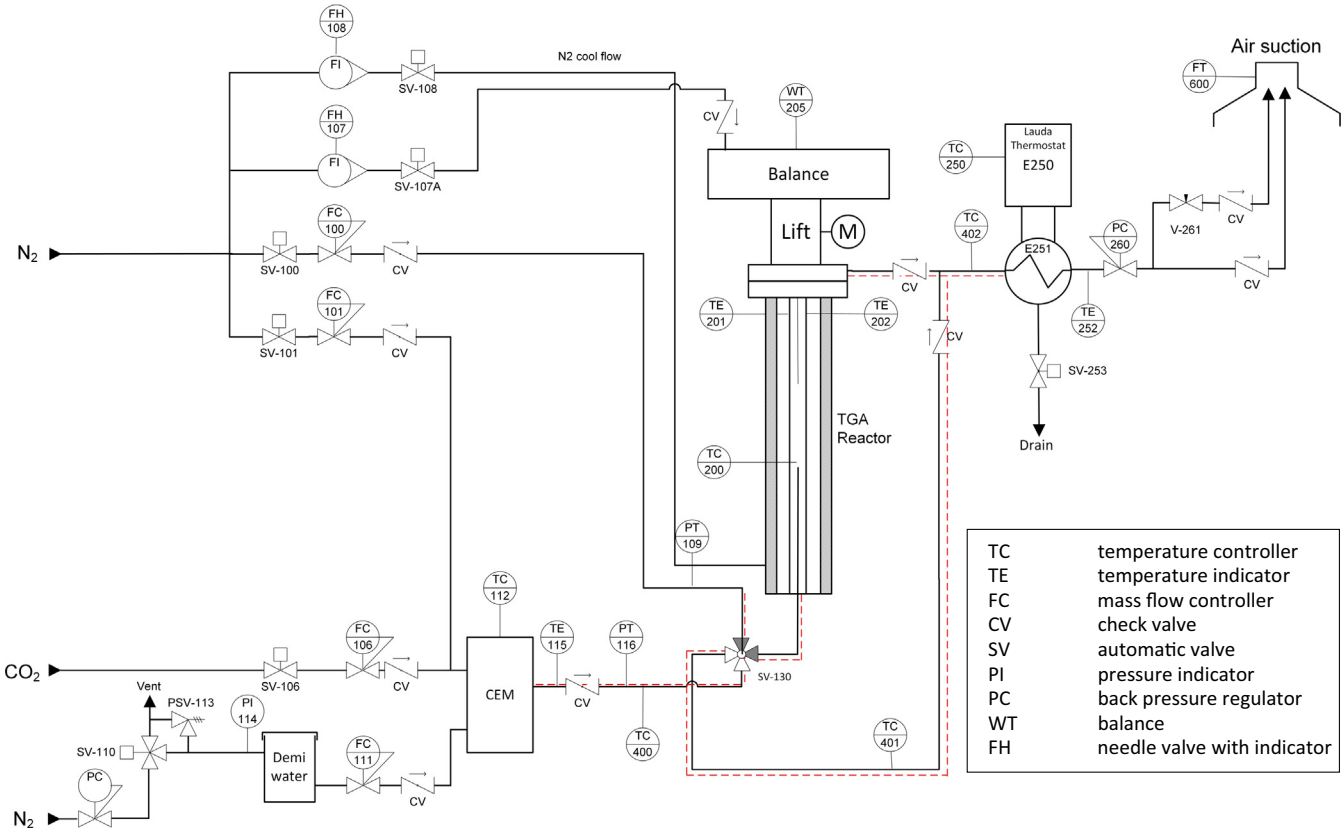

Fig. 1. P&ID of the HP-TGA setup.

TGA experiments were performed using an in-house designed setup for operation up to 10 bar (denoted as HP-TGA, Fig. 1). A microbalance (Sartorius M25D) with a sensitivity of 1 μg and 200 mg of operating range is connected to a reactor designed for TGA experiments. The maximum operating temperature of this reactor is 1100 °C. A N_2 stream is used to purge the balance and the reactor heating elements protecting them from reactive gas mixtures. The gas feeding system is equipped with Bronkhorst mass flow controllers (MFC) to produce different reactive gas mixtures, where a CEM system is installed to produce the desired quantities of steam (either with N_2 or CO_2 as carrier gas). All lines are traced and can be heated up to 450 °C to avoid steam condensation even at higher pressures. A porous ceramic basket was used with approximately 100 mg of sample mass for each experiment. At every pressure, the gas flow rate was adjusted such that mass transfer limitations due to the reduced volumetric flow rate in the reactor are avoided.

The weight change obtained from the TGA experiments to study the cyclic sorption capacity, cannot be directly attributed to specific adsorbing/desorbing species for gas mixtures in case multiple species interact with the material. TGA cycles containing different consecutive adsorption and regeneration steps with different gas compositions were designed in order to be able to link the weight change to a certain gaseous species adsorbed or desorbed. To understand the influence of steam on the adsorption of CO_2, a basic set of experiments was designed and performed in the TGA. The same steam concentration of 34% has been chosen similar as in an earlier published study [28]. CO_2 adsorption was measured with a CO_2 partial pressure of 0.66 bar. Each step in the TGA cycle has a duration of 30 min as it was established earlier that a half-cycle time of 30 min is sufficiently high to study the prevailing phenomena in the reactive system [27]. Table 1 shows the basic set of experiments performed in the TGA. One experiment consists of 2–5 different steps. In the table a step is indicated as follows: STEP1 ⇨ STEP2, where the different gases in the reactor feed are mentioned for each step. Every experiment was performed 5 times in a cyclic way, starting again with the first step, before the next experiment was conducted. The average of the last 3 measurements for every experiment is reported as cyclic sorption capacity. The sorbent cyclic capacity is based on the sample mass after the pretreatment step to minimize the effect of irreversible adsorption of CO_2.

The following terms will be used in the following sections to describe the different processes: A step is referred to as an

Table 1
Base set of experiments to study the influence of steam on the sorption capacity of KMG30 for CO_2.

Experiment number	Experimental cycle description	Steps in cycle	Total cycle time (min)
1	$H_2O/N_2 \Rightarrow N_2$	2	60
2	$CO_2 \Rightarrow N_2$	2	60
3	$CO_2 \Rightarrow N_2 \Rightarrow N_2/H_2O \Rightarrow N_2$	4	120
4	$CO_2/$ $H_2O \Rightarrow CO_2 \Rightarrow N_2 \Rightarrow N_2/$ $H_2O \Rightarrow N_2$	5	150
5	$CO_2 \Rightarrow CO_2/$ $H_2O \Rightarrow N_2 \Rightarrow N_2/H_2O \Rightarrow N_2$	5	150
6	$CO_2/H_2O \Rightarrow N_2 \Rightarrow N_2/$ $H_2O \Rightarrow N_2$	4	120
7	$CO_2/H_2O \Rightarrow N_2/H_2O$	2	60
8	$CO_2/H_2O \Rightarrow N_2/H_2O \Rightarrow N_2$	3	90
9	$N_2/H_2O \Rightarrow CO_2 \Rightarrow N_2$	3	90
10	$CO_2/H_2O \Rightarrow CO_2 \Rightarrow N_2/H_2O$	3	90
11	$CO_2/H_2O \Rightarrow N_2/H_2O \Rightarrow CO_2$	3	90
12	$CO_2 \Rightarrow H_2O$	2	60

adsorption step, if either CO_2, H_2O or both species adsorb simultaneously. In a regeneration or desorption step the feed partial pressure of the previously adsorbed species is changed to 0. We differentiate between wet and dry steps for the regeneration of adsorbed CO_2. For a wet regeneration step the partial pressure of CO_2 is reduced to 0, whereas the partial pressure for H_2O is increased to or kept at the targeted steam partial pressure. For a dry regeneration step, only N_2 is fed to the reactor. If the sorbent is exposed to N_2 after a wet desorption step, this step is defined as a drying step.

To investigate the mechanism for adsorption of CO_2 and H_2O at different temperatures the same experiments were conducted at three different temperatures with the feed gas composition shown in the Table 2. The experiment at 400 °C is defined as the base case experiment, since this experiment was conducted several times and is used to develop the mechanism for H_2O and CO_2 adsorption on KMG30.

The measured weight change of all experiments was corrected with blank experiments carried out at the same conditions. Experiments 3–6 have been started (in separate TGA experiments) one time with CO_2 and one time with H_2O to study if a first hydroxylation or dry CO_2 adsorption has a major influence on the cyclic sorption capacity. All experiments have been performed at atmospheric pressure and with a total gas flow rate of 480 N ml/min. In a previous study, the absence of external mass transfer limitations under these conditions has already been demonstrated [27].

Packed bed reactor experiments were carried out using a small packed bed reactor with a inner diameter of 27 mm and 350 mm height (AISI 316L). A distributer plate with a pore size of 40 μm was installed at a height of 50 mm from the bottom. The reactor was filled with 53.6 g of hydrotalcite sieve fraction of 1.8–3.15 mm. The effective length of the packed bed was determined being 176 mm. The reactor was installed in an electrical furnace with three separate temperature controlled sections. A multipoint thermocouple (10 measuring points at a distance of 20 mm) was installed to measure the axial temperature profile in the bed to observe temperature fronts due to sorption effects. A gas feeding system with Bronkhorst mass flow controllers and a CEM system was used in order to supply the desired gas mixtures including steam. All gas lines to the reactor were trace-heated to avoid steam condensation. The reactor could be bypassed in order to check the gas compositions before exposing the material to the gas mixture. Two independent gas analyzing systems were used to monitor the gas compositions in the outlet during the experiments. A SICK GMS 800 gas analyzer for CO_2, CO, CH_4, H_2 and O_2 was used to monitor the gas streams continuously. In order to measure the steam content in the gas streams an Agilent Technologies Cary 630 FTIR with CaF_2 windows was used together with a RED-SHIFT gas sampling system. The FTIR was calibrated prior to the experiments using the classical Lambert-Beer law in typical adsorption spectra for the gases CO_2, CH_4 and H_2O. CH_4 was used as a tracer gas during the experiments to determine the total gas flow rate in order to convert the measured gas quantities to molar flow rates. It was proved that CH_4 did not show any interaction with the material and was not reacting with steam under the considered operating conditions. A total gas flow rate of 0.5 Nl/min was used during the experiments. The used molar fractions for CO_2, H_2O and CH_4 were 0.025, 0.10 and 0.10 respectively, with a balance in N_2. Changing the gas composition was performed by bypassing the reactor for 5 min and measuring the concentration (to check the feed gas composition). After this stabilization time the feed was sent to the reactor from bottom to top while monitoring the outlet composition of the reactor for 60 min. Experiments were conducted at atmospheric pressure and 400 °C. The empty volume of the reactor and the tubing was determined previously with blank measurements to correct the breakthrough times for both the FTIR and SICK gas analyzers. The reported results in this publication are the results obtained by the FTIR gas analyzer. A process flow diagram of the setup is given in Fig. 2.

Table 2
Experimental conditions during different experiments. Bold values are for the base case.

Temperature °C	CO_2 fraction (–)	H_2O fraction (–)	Total pressure (bar)
300	0.66	0.34	1
400	**0.66**	**0.34**	**1**
500	0.66	0.34	1

3. Results and discussion

3.1. Introduction and data representation

Before the first adsorption-desorption cycle with steam (according to Table 1), the sample was pretreated at 600 °C under a N_2 flow for 2 h. This pre-treatment was sufficient to desorb CO_2 and H_2O from the material, which was adsorbed during storage [27]. For TGA measurements the cyclic working capacity (cwc) is defined according to

$$cwc_{site} = \frac{abs(\Delta m)_{(ads)} + abs(\Delta m)_{(des)}}{2 * m_{sample(pretreated)}}$$

This cwc was determined for each adsorption/desorption step using the obtained mass change average over the last three consecutive experiments. Note that we use the mass-based cyclic working capacity, as the TGA does not provide information on the species absorbed/desorbed.

In order to prepare the reader for the following sections where the experimental results are described in detail, this paragraph briefly summarizes the main findings which had led to the detailed experimental TGA and packed bed experiments described before. The adsorption of CO_2 and regeneration with N_2 had been studied in detail in the past together with the adsorption and desorption of H_2O, where we had found a relatively low cyclic working capacity of the adsorbent. In this study we have used H_2O and CO_2 together in one cycle. Once we were introducing H_2O we found that the CO_2 adsorption capacity in the next cycle was significantly increased. Experiments in a packed bed reactor showed that during the adsorption step of CO_2, the sorbent releases H_2O. Therefore we were anticipating that CO_2 can replace previously adsorbed H_2O. Based on these experimental results we assumed that at least two different sites are involved in the mechanism for CO_2 adsorption on KMG30. One site can be regenerated when feeding only N_2 (weaker bonding of CO_2 to the adsorbent) and one site which can only be regenerated if H_2O is present during one of the regeneration steps (second site which probably involves a stronger bonding of CO_2 to the sorbent). In a last step we were trying to explain multiple experiments conducted in both the TGA and PBR. However, when considering three adsorption sites we still could not explain the experimental results completely. If CO_2 and H_2O is fed together to the sorbent, the cyclic working capacity for CO_2 was significantly increased. To be able to describe these experimental findings a third site for CO_2 was needed, that is active after the sorbent was previously exposed to CO_2 and H_2O simultaneously. Adding this site to our model all the experimental findings from the TGA and PBR could be described and explained.

In the following section we will explain the development of the mechanism for both CO_2 and H_2O step by step based on the results from the different experiments performed in the TGA and PBR. Note that the conditions of the experiments carried out in the

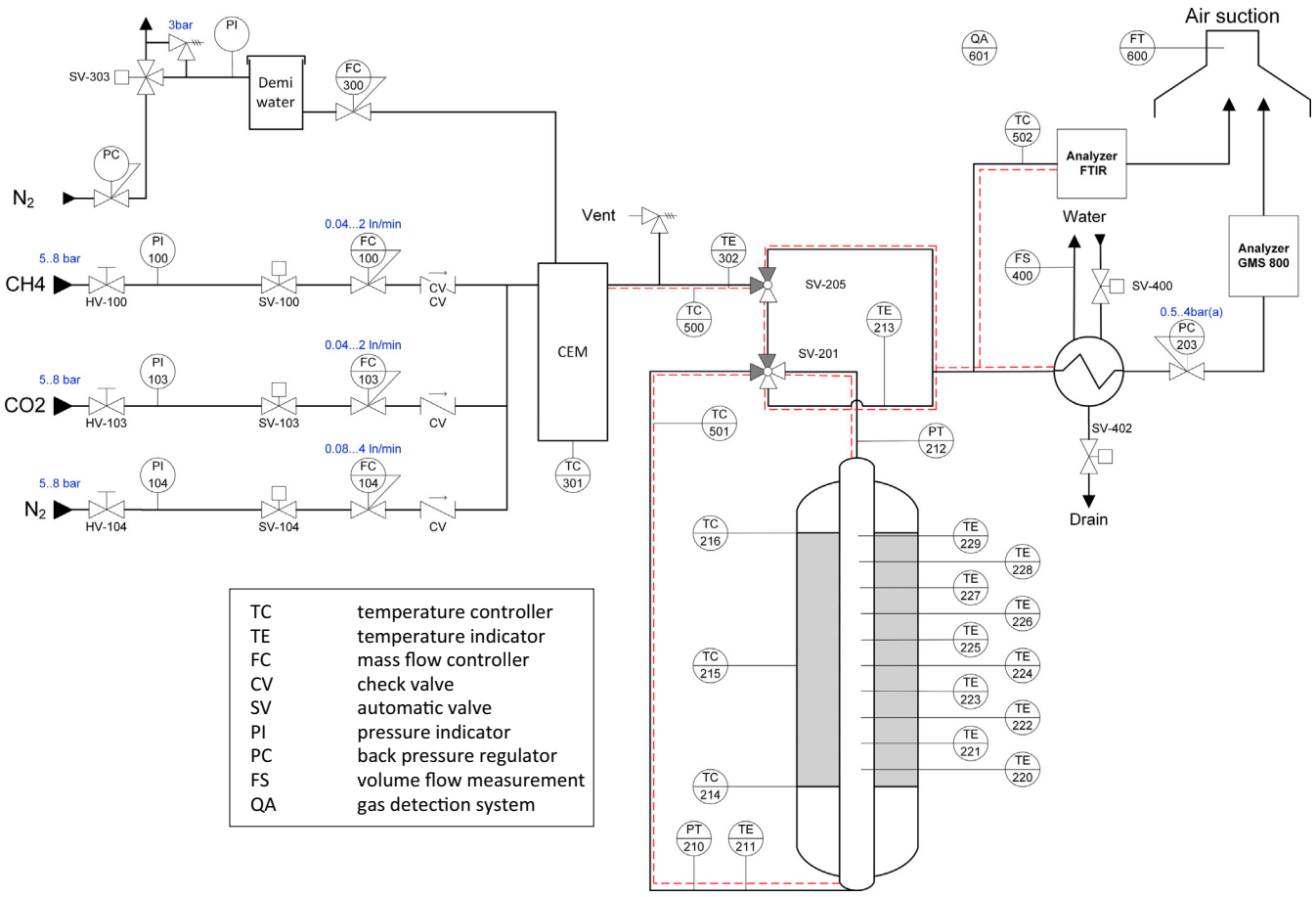

Fig. 2. P&ID of packed the bed reactor for the breakthrough experiments.

PBR are different from the conditions used in the TGA. Because of this and the different dynamic behavior of a PBR compared to a TGA, we compare the experimental results from the packed bed reactor only qualitatively to those obtained from the TGA experiments. In the following section we will show the results in the following two different types of figures.

3.1.1. TGA

Arrows are used in the figures that show the normalized weight change as a function of time to indicate which sites are involved in the adsorption/desorption steps, where the mass at the start and end of each step is indicated by a dotted line. Two different colors are used for the arrows. Red arrows represent the mass of CO_2 exchanged in one experimental step, whereas blue arrows represent the mass of H_2O exchange. The total height of the arrow represents the total mass change obtained in the experimental step and the contributions for the different sites are indicated by their letter. An increase in the adsorbate content is represented by a solid arrow, a decrease by a shaded arrow. An example for a representation of three different sites involved in an adsorption step can be found in Fig. 3.

3.1.2. PBR

The areas in the figures (integration of analyzer signal over the time with respect to the baseline) are colored in the same way as for the TGA results, see Fig. 3. The signal for CO_2 and the corresponding areas are plotted in red, whereas the signal and areas for H_2O are plotted in blue. Again we distinguish between adsorption (solid area above the signal) and desorption (shaded area below the analyzer signal).

3.2. Development of the mechanism based on the experimental results

3.2.1. Adsorption of H_2O on KGM30

The normalized weight change of an adsorption experiment of water is plotted in Fig. 4a. The first cycle shows a larger mass change than the subsequent steps, which is consistent with earlier published results [27]. The cyclic working capacity of H_2O was determined on the basis of the last cycle and amounted to 8 mg/g. Very similar results were obtained when analyzing the amount of H_2O adsorbed during the PBR experiments. Also in this case the first cycle showed a somewhat higher adsorption capacity than the subsequent steps (Fig. 4b). In order to describe the cyclic working capacity on the adsorbent we call the adsorption site for H_2O Site A.

3.2.2. Adsorption of CO_2 on KMG30

Fig. 5a shows results of a similar experiment with CO_2 as the adsorbate. As for water adsorption, both the TGA as the PBR CO_2 experiments showed a higher adsorption capacity for the first cycle and similar CO_2 cyclic working capacities of 12 mg/g. In a previous study, we have already reported that the measured cyclic working capacity is mainly determined by the desorption time [27], i.e. the longer the desorption time step, the higher the cyclic working capacity for both CO_2 and H_2O. For the settings used in this experiments we will call the site where CO_2 can be adsorbed and desorbed with N_2, site B. Thus far the adsorbent was exposed to either CO_2 or H_2O in a cyclic manner, the cycles presented in the next sections contain steps where CO_2 and H_2O are combined. It will become apparent that the sorbent behavior when both steam

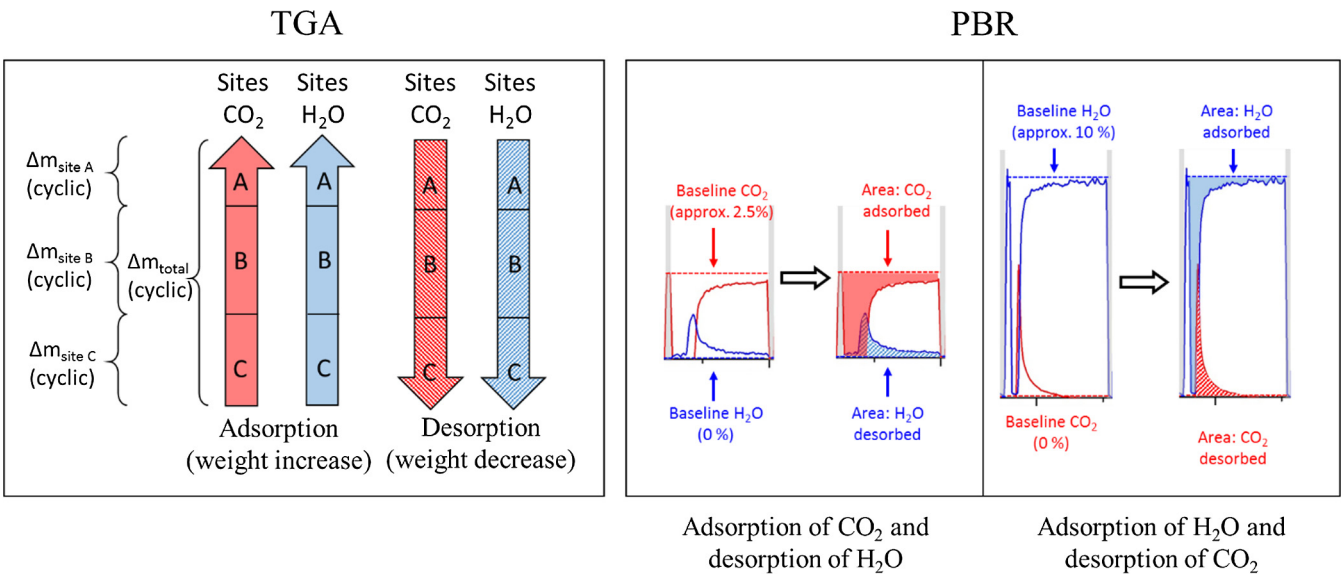

Fig. 3. Visualizations used in the figures to explain the different sites involved in CO_2 and H_2O adsorption on KMG30.

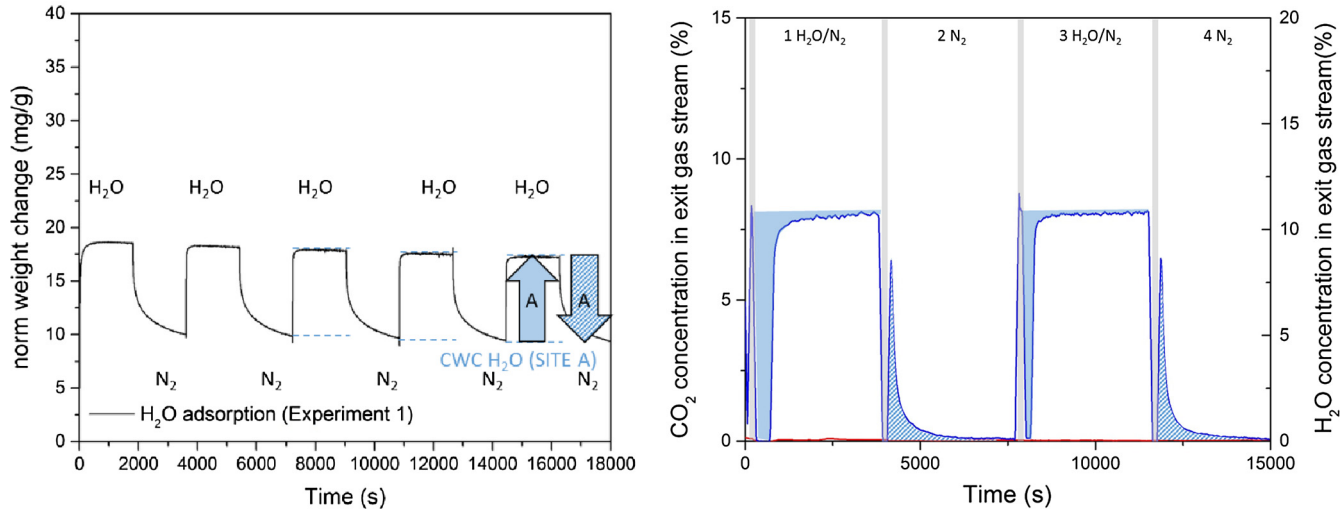

Fig. 4. (a) TGA Experiment 1: adsorption/desorption of H_2O at 400 °C and PH_2O = 0.34 bar (b) PBR Experiment 1 at 400 °C and PH_2O = 0.1 bar.

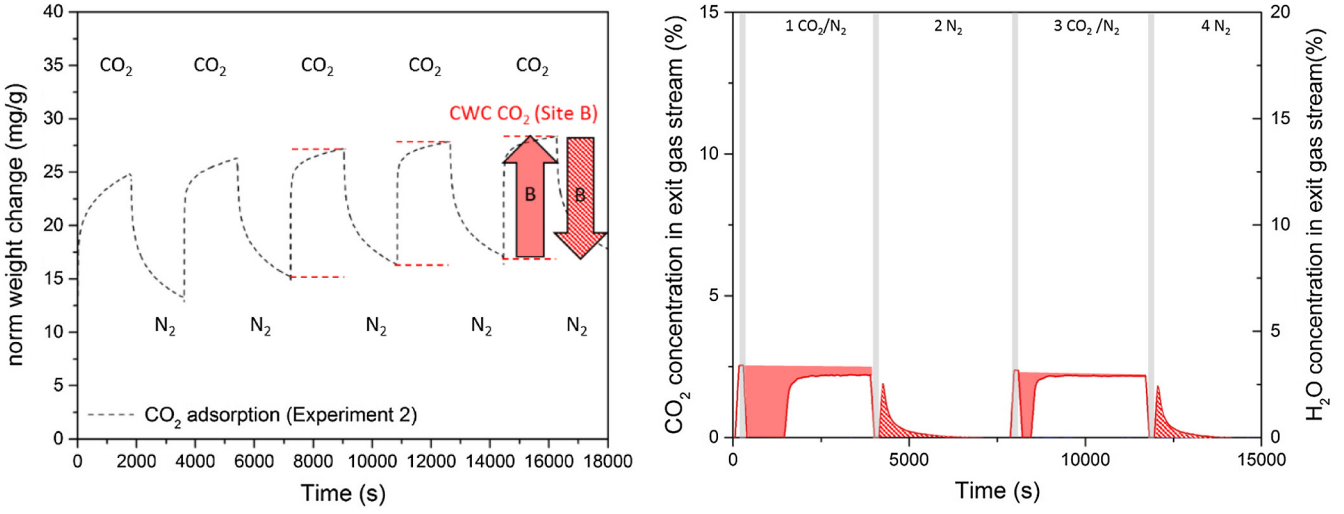

Fig. 5. (a) TGA experiment 2: adsorption/desorption of CO_2 at 400 °C and PCO_2 = 0.66 bar (b) PBR Experiment 2 at 400 °C and PCO_2 = 0.025 bar.

and CO_2 are present in the cycle cannot be described by a single site A for steam and a single site B for CO_2.

3.2.3. Combination of CO_2 and H_2O in one cycle on KMG30

Fig. 6a shows the normalized weight changed measured during the first cycle of Experiment 3 to illustrate the mechanism of CO_2/H_2O interaction on the material. Prior to this Experiment 3, Experiment 2 was conducted and accordingly the starting weight in this graph represents the adsorbed amount of 12 mg/g of CO_2 assigned to site B of Experiment 2. The subsequent regeneration step with N_2 desorbs this amount of CO_2. If only two sites (A for H_2O and B for CO_2) would be present, the subsequent H_2O feeding in step 2 would result in an increase of 8 mg/g due to water adsorption in the TGA experiment. However, a first rapid weight increase followed by a slow decrease in weight is observed. In the PBR experiment, besides water adsorption, desorption of CO_2 is observed. It appears that the adsorption of H_2O results in a release of CO_2 that was still adsorbed after the previous steps. The following desorption step with N_2 (step 3) induces water desorption of 8 mg/g as already observed in Experiment 1. In the PBR experiment, indeed only a response for water desorption is observed. Once the material is again exposed to CO_2 (step 4), adsorption of CO_2 is apparent both in the TGA as the PBR experiment. The amount of CO_2 adsorbed, however, is higher than the measured cyclic weight change in the CO_2-only Experiment 2 (Site B, Fig. 5a) and it is similar to the CO_2 amount adsorbed in the first adsorption step of Experiment 2 (Fig. 5a).

Based on these observations it appears that steam adsorption during step 2 induces desorption of CO_2, resulting in the measured net weight decrease as measured in the TGA experiment and the CO_2 response measured in the PBR experiment. We propose that this adsorbed CO_2 must be assigned to a second site for CO_2 (Site C) which can be regenerated by H_2O adsorption but not by N_2 flushing. Indeed, when comparing the TGA cycles with the packed bed test (Fig. 6b), it is evident that in step 2 in the packed bed reactor experiments the adsorption of water also results in a desorption of CO_2. Thus the existence of Site C is confirmed.

Experiment 3 was performed twice: once staring with steam adsorption as the first step and once with CO_2 adsorption as the first step. In Fig. 7, the TGA results are shown for the two experiments, synchronized in time so that the two CO_2 adsorption steps start at the same moment. As can be seen, the obtained weight changes are identical for both experiments (i.e. dashed red line and the solid black line are on top of one another). For the experiment starting with H_2O, H_2O adsorption and desorption on site A according to Experiment 1 is observed. The steam desorption is incomplete and there is still water present on the material. Since it is known that all water desorbs during the CO_2 adsorption step (from the experiments in the packed bed reactor), it can be concluded that 7.5 mg/g of water is still present before the step with CO_2 (site C on the blue arrow) is started. This amount of water is replaced by CO_2 and additional CO_2 is adsorbed as it is known from Experiment 2 in step 3 (Fig. 5a). For the experiment where the adsorbent was not exposed to H_2O only CO_2 is adsorbed. Since the obtained weight changes are identical in the following steps it can be assumed that the adsorbent is in the same state at this point. To explain these experimental results we can assume the presence of a metal oxide site that can be either transformed into hydroxide (when water is present) or into carbonate (when CO_2 is present). Note that we assume in this case that the equilibrium is shifted completely, which will depend on the partial pressure used during the experiments, since the formation hydroxide and carbonate is determined by an equilibrium.

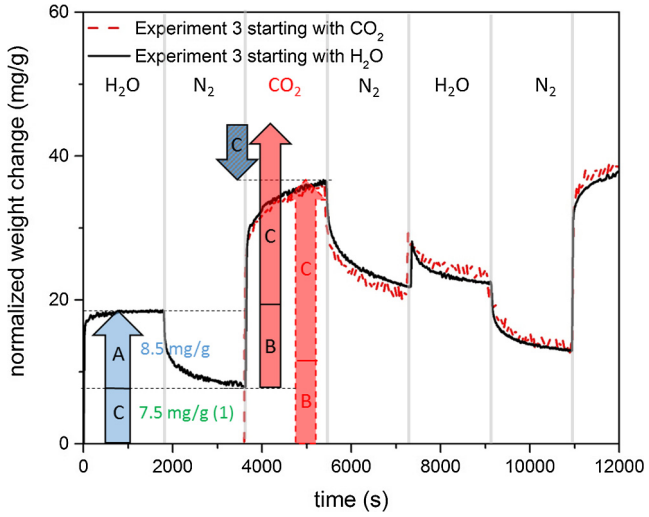

Fig. 7. TGA Experiment 3 starting with H_2O and CO_2 measured at 400 °C and PH_2O = 0.34 bar PCO_2 = 1.

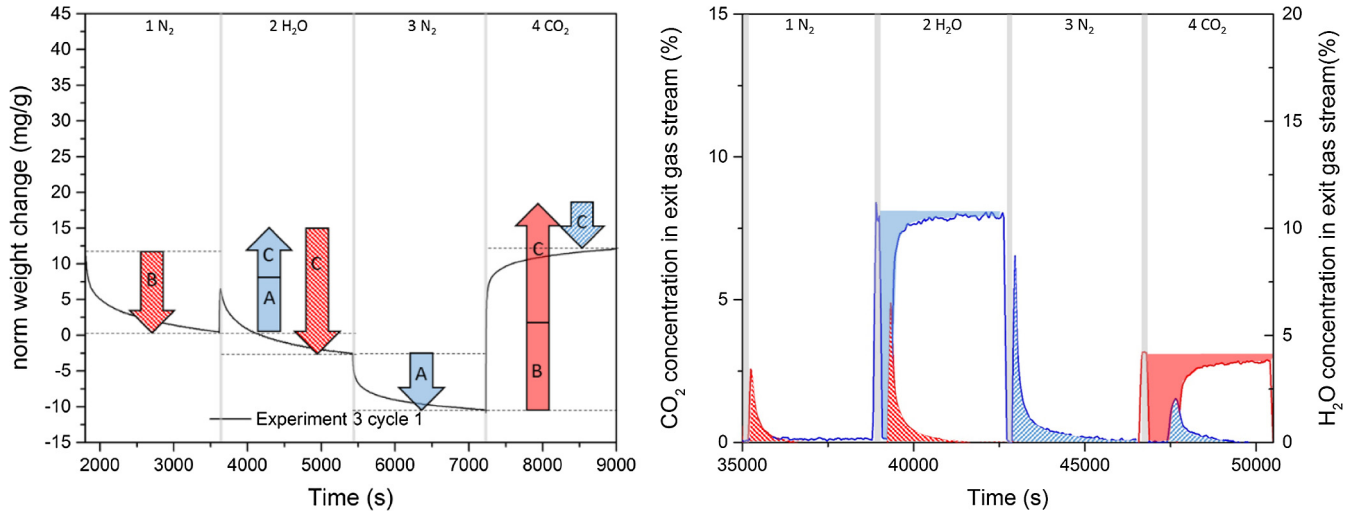

Fig. 6. (a) TGA Experiment 3: adsorption of CO_2 with dry (N_2) and wet regeneration (H_2O) at 400 °C and PH_2O = 0.34 bar PCO_2 = 0.66 bar (b) PBR Experiment 3 at 400 °C and PH_2O = 0.1 bar PCO_2 = 0.025 bar.

Assuming a general metal oxide forming a metal hydroxide or carbonate, the following reactions can occur, depending on the gas phase composition:

$$C[\bullet]O + H_2O \rightarrow C[(OH)_2] \quad 7.5\ \text{mg/g}(0.416\ \text{mmol/g}) \tag{1}$$

$$C[(OH)_2] + CO_2 \Longleftrightarrow C[CO_3] + H_2O \quad 11\ \text{mg/g}(0.416\ \text{mmol/g}) \tag{2}$$

$$C[\bullet]O + CO_2 \rightarrow C[CO_3] \quad 18.5\ d\text{mg/g}(0.416\,\text{mmol/g}) \tag{3}$$

Based on the observed additional mass increase of 7.5 mg/g of water for Site C, the amount of moles of water in this hydroxide is 0.416 mmol/g of H_2O. Assuming equimolar exchange between CO_2 and H_2O, the expected mass change would be approx. 11 mg/g if the sorbent transforms these sites from a hydroxide to a carbonate (Eq. (2)) and approx. 18.5 mg/g if the sorbent directly transforms from a metal oxide into a carbonate (Eq. (3)) during a dry CO_2 feed. Note that reactions 1 and 3 are only occurring during the first time the material is exposed either to H_2O (reaction 1) or to CO_2 (reaction 3) after the pretreatment. After the activation of this site, the hydroxide can only be transformed with CO_2 to a carbonate and vice versa. It can be inferred from Figs. 6 and 7 that our assumption can describe the obtained weight changes during the two different experiments quite well.

3.2.4. Mixed adsorption of CO_2 and H_2O in one step on KMG30

During this experiment the material is first exposed to CO_2/H_2O (step 1) followed by an exposure to a dry CO_2 stream (second step). Fig. 8b (breakthrough curves) shows that, when switching from a wet to a dry CO_2 gas stream, H_2O desorbs as one would expect while CO_2 adsorbs although the CO_2 partial feed pressure does not change (step 2). The CO_2 adsorbing during this step can be ascribed to shifting of the equilibrium between the metal hydroxide and the metal carbonate of site C: the hydroxide is completely transformed into a carbonate, adsorbing CO_2 and releasing H_2O. Note that the loading of site B remains unchanged. Illustratively, in the subsequent step with N_2 (step 3 of the breakthrough experiment) no H_2O desorption is observed indicating that the additional CO_2 adsorption in step 2 results in a fully dry sorbent. This means that in step 2, all water from site A (8 mg/g) and all water present due to the equilibrium reaction of site C (derived from Eq. (2)) is released.

In this step 2 the mass change detected by the TGA is a loss of 2 mg/g. While steam desorption of site A corresponds to decrease of 8 mg/g, it means that the shift in equilibrium on site C due to Eq. (2) corresponds to a mass increase of 6 mg/g as illustrated in Eq. (4):

$$-8\frac{\text{mg}}{\text{g}}[A] + 6\frac{\text{mg}}{\text{g}}[C] = -2\frac{\text{mg}}{\text{g}}[measured] \tag{4}$$

The mass change of 6 mg/g would correspond to an exchange of 0.23 mmol/g hydroxide to carbonate of site C. This also implies that in step 1 due to the equilibrium reaction (2) 0.186 mmol/g of site C was already occupied by CO_2.

Summarizing for step 1, the mass increase due to adsorption expected should thus be 8 mg/g of H_2O for site A, 12 mg/g of CO_2 for site B, and of 4.8 mg/g for site C as explained above. A total mass change of approximately 25 mg/g is thus expected. However, the measured mass change during this step equals 31 mg/g. Thus, an additional site should be present in the sorbent, denoted in this work as site D and responsible for a 6 mg/g mass change in step 1. Since in step 2 the exchange of water can be explained with sites A, B and C, and since in step 3 (Fig. 8b) there is no water desorption, it appears that site D is able to only adsorb CO_2. Additionally, as this site was not present in the previous experiments, we conclude that this site is only available when the sorbent is sufficiently hydroxylated and exposed to CO_2. Indeed it was observed that during the first exposure to a mixture containing both CO_2 and H_2O simultaneously, a significantly higher mass increase was detected in the TGA experiments, which is attributed to the activation of this site D (Fig. 8a, Experiment 4 cycle 1). If this hypothesis is true, we should measure additional CO_2 desorbing in the following steps compared with the three sites theory.

Step 2 resulted in complete water desorption as discussed above. The mass change in the subsequent step 3 (desorption with N_2), desorption of CO_2 should only occur from site B in case only site A, B and C are assumed, corresponding to a mass change of 12 mg/g. The observed mass change is, however, higher (around 15 mg/g) and the sorbate desorbed is only CO_2 as evidenced by the packed bed experiment. So, the additional CO_2 should be released by site D in this step. However, the mass exchange is only about 50% of the CO_2 adsorbed on site D in step 1. Thus, more CO_2 is expected to be released in the next step.

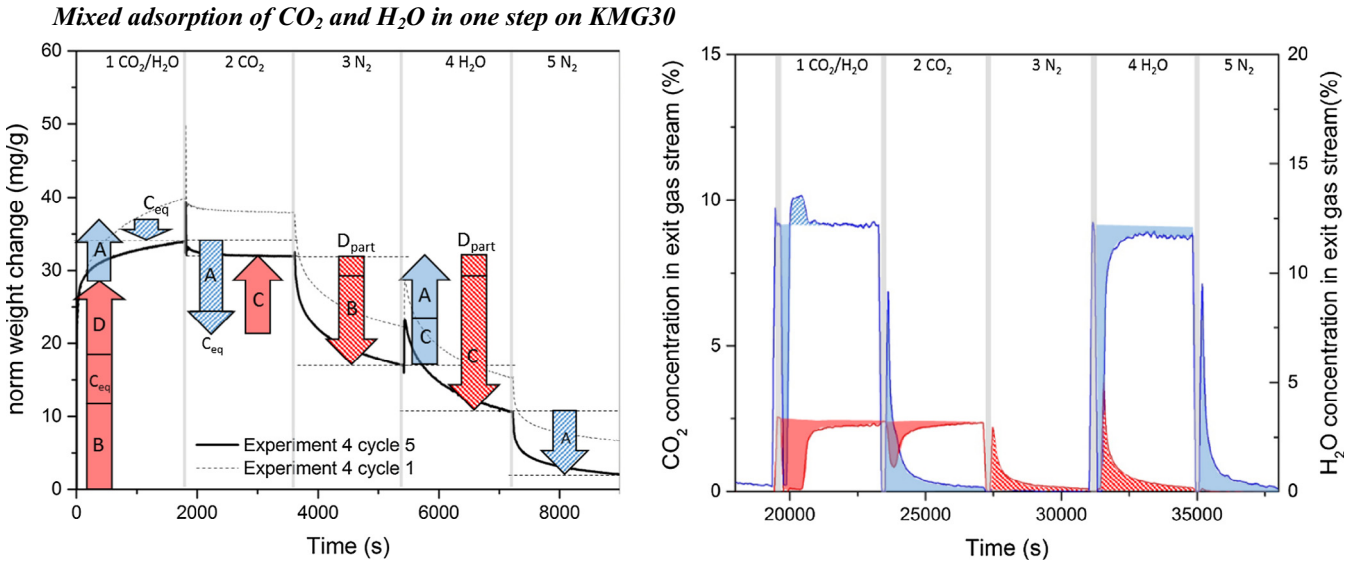

Fig. 8. (a) TGA Experiment 4: adsorption of CO_2/H_2O followed by CO_2 and desorption with dry (N_2) and wet regeneration (H_2O) at 400 °C and PH_2O = 0.34 bar and PCO_2 = 0.66 bar (b) PBR Experiment 4 at 400 °C and PH_2O = 0.1 bar and PCO_2 = 0.025 bar.

Indeed, when analyzing step 4, according to the three sites theory, one would expect adsorption of water on site A (8 mg/g) and an exchange of carbonate to hydroxide according to Eq. (2), which would correspond to a weight loss of 11 mg/g, so that in total one would expect a weight decrease of 3 mg/g. However, the measured weight loss in this step is 6 mg/g, which confirms that the rest of site D is released during this step. The next step (desorption with N_2) at this point should only desorb water present on site A, which is indeed confirmed by the observed mass loss corresponding to 8 mg/g.

3.2.5. Mixed adsorption of CO_2 and H_2O in one cycle on KMG30

In the discussion of the following experiments, it will be confirmed that the experimental observations can indeed be adequately described by the proposed four site mechanism.

Experiment 5 is very similar to Experiment 4, but steps 1 and 2 are reversed. The results for Experiment 5 have been plotted in Fig. 9 for both TGA (a) and PBR (b). Step 1 of Experiment 5 is the same as step 4 of Experiment 3 (see Fig. 6) and can be described in the same way with the four sites theory: site B adsorbs CO_2 and site C is transformed from a hydroxide into a carbonate, resulting in CO_2 adsorption and H_2O desorption. In the second step (wet adsorption) CO_2 is desorbing due to the shift in equilibrium of site C (Eq. (2)) which leads to a mass decrease of approx. 6 mg/g. Additionally, site D is occupied again with CO_2 and site A with H_2O. The next step 3 with N_2 flushing only leads to desorption of CO_2 from site A and H_2O from site B, while site C and site D are unaffected since they can only be desorbed if H_2O is present in the feed. The adsorbing water in step 4 in the absence of CO_2 in the feed causes site D to release its adsorbed CO_2. Compared to step 4 of Experiment 4, the amount of CO_2 released in step 4 of Experiment 5 is smaller, since step 2 of Experiment 5 results in a lower equilibrium amount of CO_2 on site C than step 2 in Experiment 4 because of the presence of H_2O in the feed during step 2 in Experiment 5.

The results of Experiment 6 have been plotted in Fig. 10 for the TGA and PBR experiments. It differs from Experiments 4 and 5 in that the step with adsorption in dry CO_2 conditions is not performed. This implies, that the total capacity of Site C cannot be reached in this experiment. It can be seen from Fig. 10a that indeed the measured mass change from the TGA can be described with the proposed four sites mechanism. The mass change in the first step is similar to the mass change in step 1 of Experiment 4 (see Fig. 8a) and the rest of the steps are similar to the results obtained in Experiment 5. The same observation are made for the results of the PBR which shows similar evolution of measured outlet concentrations compared to the previous experiments.

In Experiment 7 (see Fig. 11) the material was exposed continuously to steam at a constant partial pressure, while CO_2 is periodically added to the feed. Following the proposed mechanism, sites B, D and C (equilibrium) are adsorbing CO_2 and are regenerated in the subsequent step (note that site B does not require H_2O to desorb CO_2). The effects of Site C, on which both H_2O and CO_2 can adsorb, is clearly observed in the results of the packed bed experiments, since desorption of H_2O upon adsorption of CO_2 and adsorption of H_2O upon desorption of CO_2 is observed. In this experiment Site C alternates between fully hydroxide and equilibrium loaded hydroxide/carbonate. The breakthrough times for CO_2 for both experiments (Experiment 6 and Experiment 7) were nearly equal which is expected in accordance with the developed mechanism.

To confirm that site A for H_2O is always fully occupied in this experiment, Experiment 8 is performed having an additional drying step, see Fig. 12 solid line). It can be seen that indeed the expected mass is lost in Experiment 8 (Step 3) due to the water desorption. The mass increase during the following adsorption cycle is equal to the mass increase, which was measured during the first step of Experiment 7 and Experiment 8 where the material was previously dried. Moreover, this figure nicely shows in which way the cyclic obtained mass change is the same for different cycles performed, if the conditions are the same.

Fig. 13(a–d) shows additional experiments which were conducted to prove the developed mechanism and the introduced adsorption sites for KMG30. First of all one can notice, that the four sites mechanism is able to predict the mass change which was measured during Experiment 9 to Experiment 12. Secondly, we can confirm the hypothesis, which was introduced previously, that site D will only be partly filled and emptied with CO_2 in case dry CO_2 is fed. To reach full capacity of site D a step with CO_2/H_2O is necessary. Small deviations in the measured cyclic weight change can be expected due the different sites between experiments with a higher number of desorption/regeneration steps as the total desorption time is different in these experiments [27].

Based on the experimental results described above the model proposed for the adsorption of CO_2 and H_2O on KMG30 is summarized in Fig. 14 together with the cyclic working capacity of the sites summarized in Table 3.

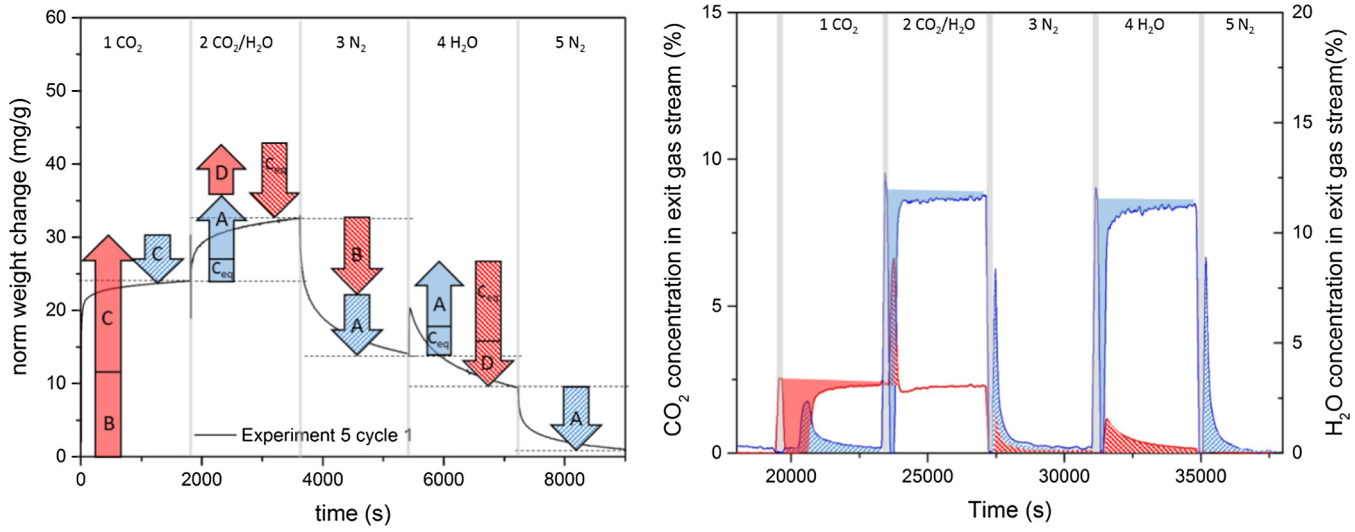

Fig. 9. (a) TGA Experiment 5: adsorption of CO_2 followed by CO_2/H_2O and desorption with dry (N_2) and wet regeneration (H_2O) at 400 °C and PH_2O = 0.34 bar PCO_2 = 0.66 bar (b) PBR Experiment 5 at 400 °C and PH_2O = 0.1 bar and PCO_2 = 0.025 bar.

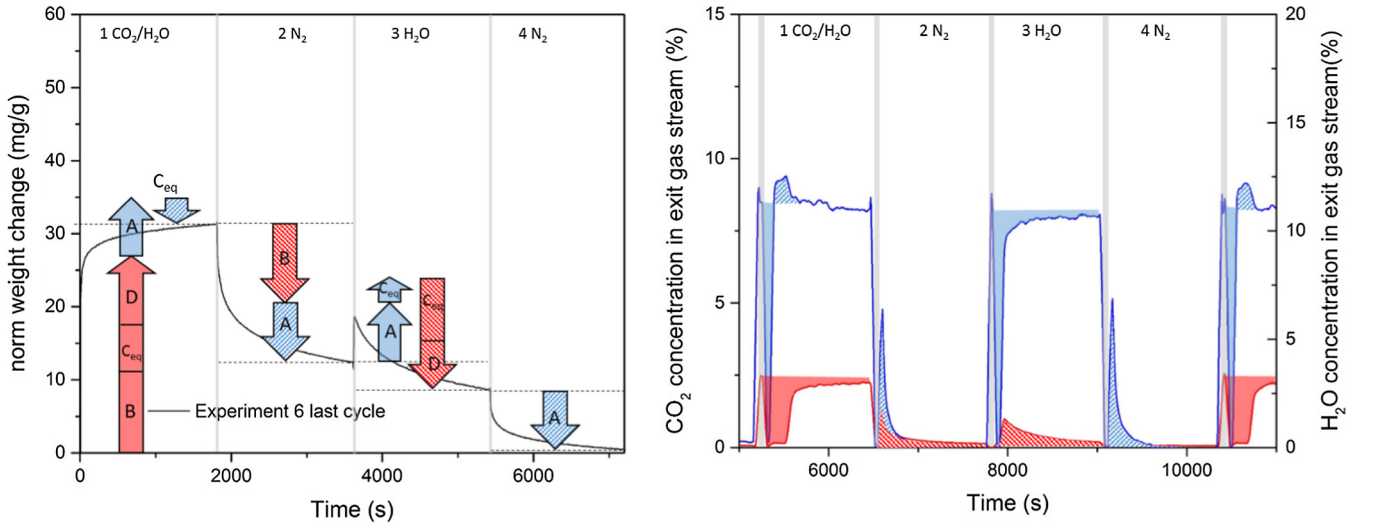

Fig. 10. (a) TGA Experiment 6: adsorption of CO_2/H_2O and desorption with dry (N_2) and wet regeneration (H_2O) at 400 °C and PH_2O = 0.34 bar and PCO_2 = 0.66 bar (b) PBR Experiment 6 at 400 °C and PH_2O = 0.1 bar and PCO_2 = 0.025 bar.

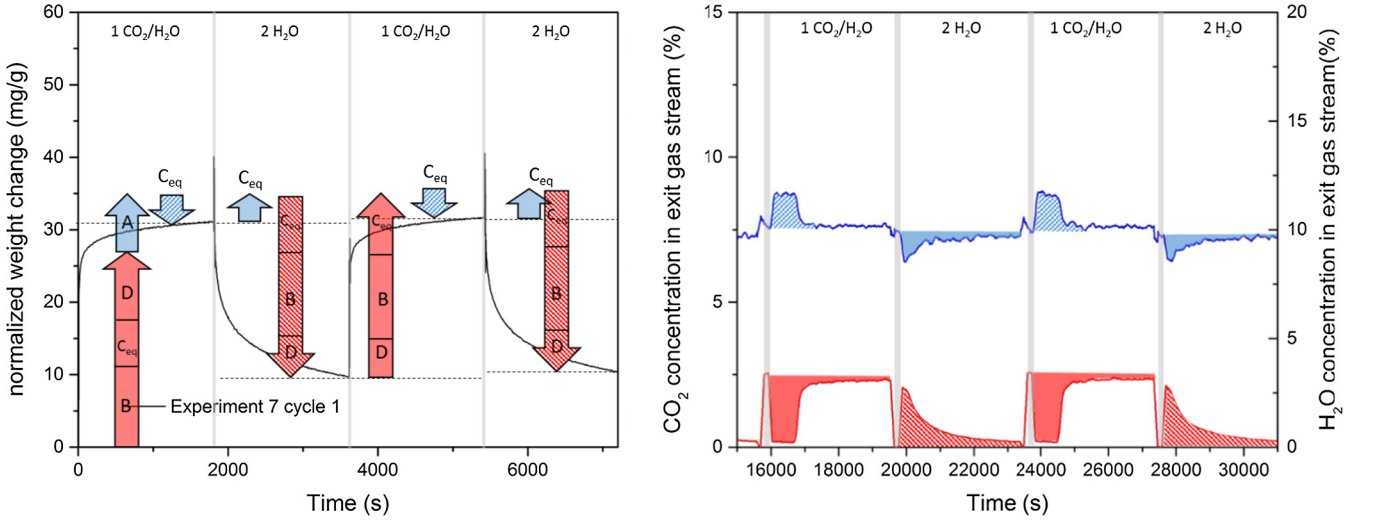

Fig. 11. (a) TGA Experiment 7: adsorption of CO_2/H_2O and wet regeneration (H_2O) at 400 °C and PH_2O = 0.34 bar and PCO_2 = 0.66 bar (b) PBR Experiment 7 at 400 °C and PH_2O = 0.1 bar and PCO_2 = 0.025 bar.

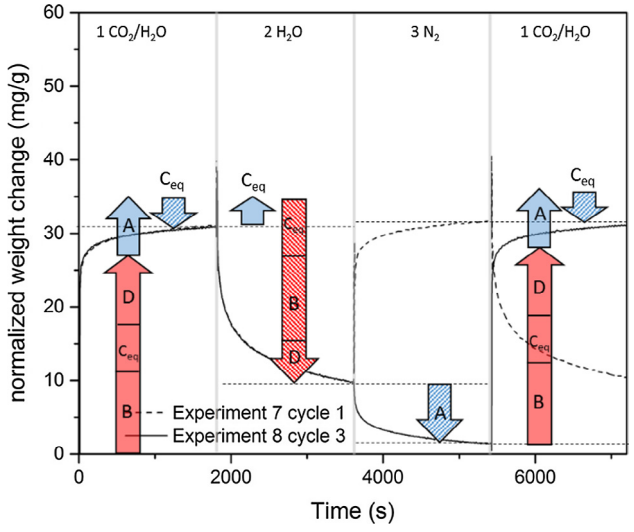

Fig. 12. TGA Experiment 8: adsorption of CO_2/H_2O, wet regeneration (H_2O) and drying (N_2) at 400 °C and PH_2O = 0.34 bar PCO_2 = 0.66 bar compared to the TGA experiment 7.

According to this model, site A for H_2O sorption (0.28 mmol/g) and site B for CO_2 sorption (0.3 mmol/g) are active after the pre-treatment of the sorbent. Their behavior is already described in the literature at different temperatures and adsorption/desorption times and both can be regenerated with N_2 [27]. Site D for CO_2 sorption, however, needs to be activated. This site in only capable of CO_2 adsorption if the material contains adsorbed H_2O and is active after the first time when CO_2 and H_2O was fed together to the material. This can result from simultaneous feeding CO_2 and H_2O, or by preventing full steam desorption in the preceding step to feeding dry CO_2. The full capacity of this site is probably much higher than its cyclic working capacity (0.14 mmol/g). This site can be responsible for the in general slightly higher CO_2 cyclic working capacities which are reported in the literature for experiments were steam was present during the adsorption step [25,26,29]. Site C can adsorb both CO_2 as H_2O and has a high CO_2 cyclic working capacity (0.42 mmol/g for dry CO_2). If CO_2 and H_2O are present together in the feed stream, an equilibrium will be established which leads to a replacement effect of CO_2 or H_2O dependent on the feed composition. Note that we need site D in order to predict the cyclic working capacities for this material for

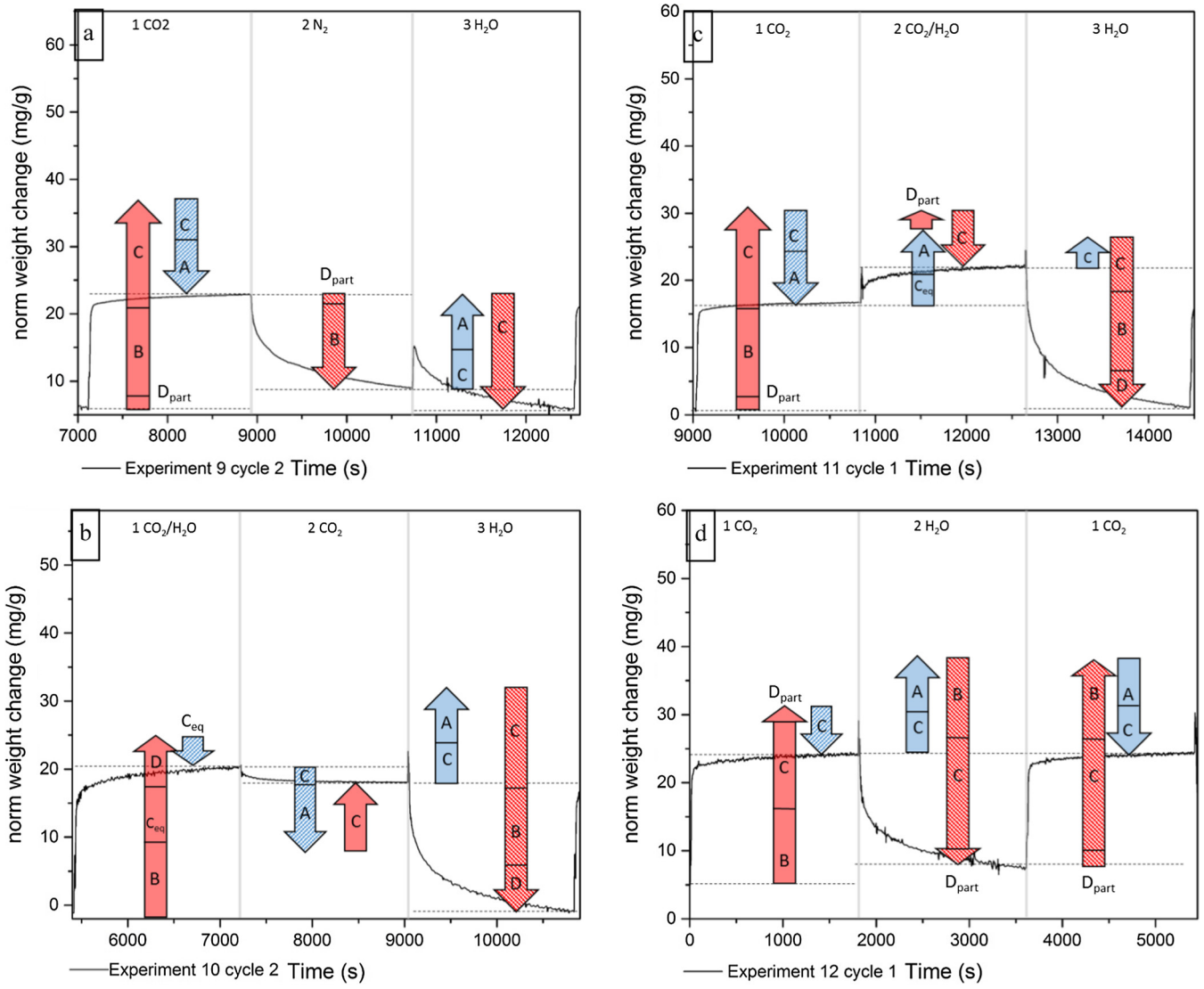

Fig. 13. a–d: TGA results of Experiments 9–12 conducted at 400 °C, PH_2O = 0.34 bar and PCO_2 = 0.66 bar to support the developed mechanism for the CO_2/H_2O interaction on KMG30.

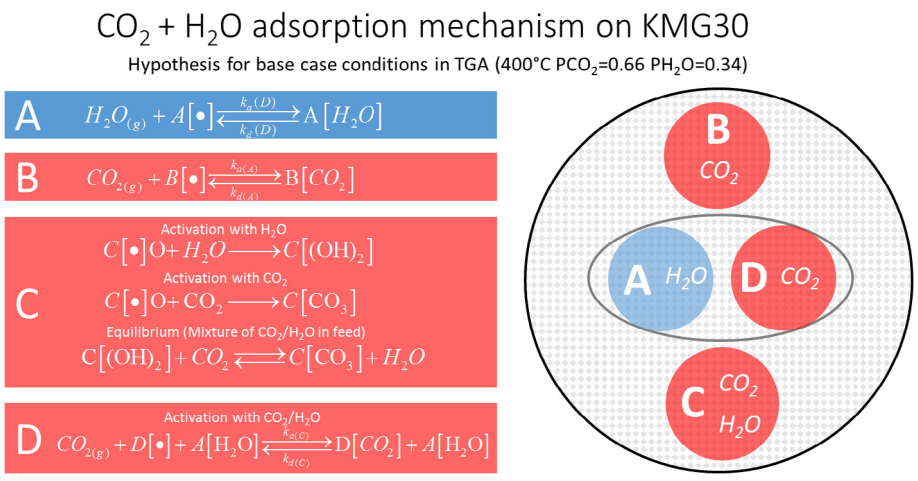

Fig. 14. Proposed model for CO_2 and H_2O adsorption on KGM30 at 400 °C.

Table 3
Cyclic working capacities of the different sites at 400 °C at PCO_2 = 0.66 bar and PH_2O = 0.34 bar.

Site	Adsorbate	Regeneration conditions	Cyclic working capacity		Description
			mg/g	mmol/g	
A	H_2O	Dry	5	0.28	Always active
B	CO_2	Dry	12 (13)	0.30	Always active (increased capacity after first time CO_2/H_2O)
D	CO_2	Wet	6	0.14	activated after first time exposed to CO_2/H_2O
C	H_2O	CO_2	7.5	0.42	H_2O feed
	CO_2	H_2O	18.5	0.42	dry CO_2 feed
C_{eq}	CO_2	H_2O	4.5	0.10	CO_2/H_2O feed
	H_2O	CO_2	5.7	0.32	
CO_2 cyclic working capacity (only dry reg.)				0.30	dry CO_2 feed
CO_2 cyclic working capacity (wet reg.)				0.72	dry CO_2 feed
CO_2 cyclic working capacity at equilibrium				0.53	CO_2/H_2O feed
CO_2 cyclic working capacity with dry CO_2 feed				0.85	dry CO_2 feed after CO_2/H_2O

Table 4
Possible species formed on potassium promoted hydrotalcite proposed in the literature.

Species	Name	Conditions	Refs.
$KAlCO_3(OH)_2$	Dawsonite	10 bar CO_2 steam at 200 °C	[31]
K_2CO_3/K-O-Al (OH)y/AlOOH-Al_2O_3	Hydroxyalumina centers		
K_4H_2 $(CO_3)_3 \times 1.5$ H_2O	Potassium carbonate hydrate	Different temperature CO_2 and H_2O up to 600 °C	[26]
$K_2Mg(CO_3)_2$	Potassium magnesium carbonate		
$KAlCO_3(OH)_2$	Dawsonite		
$Mg(OH)_2$	Brucite		
MgO	Magnesium oxide		
$Mg_6Al_2K_2O_{10}$	–	250–500 °C at 980 Torr	[7]
$MgAl_2K_2O_9(CO_3)$	–		
$MgAl_2K_2(CO_3)_2$	–		
$Mg(OH)_2$	Brucite	Up to 400 °C and 1.52 MPa CO_2	[30]
$MgCO_3$	Magnesium carbonate		
$K_2Al_2O_4$ 3 × H_2O	Potassium aluminum oxide hydrate	Different temperature CO_2 and H_2O up to 600 °C	[32]

all conditions (history of the material). However, this does not necessarily mean that site D is a separate physical site. It has to be considered that the additional CO_2 adsorbed by site D could also be explained by the activation of additional cyclic working capacity for sites B and C after feeding H_2O and CO_2. Also in this way the experimental results published here could be explained

In order to enlighten the chemical nature of the different sites proposed in this publication earlier published studies were investigated. However, in the literature various chemical species have been proposed being responsible for the CO_2 adsorption mechanism and are summarized in Table 4. Even though $MgCO_3$ formation from brucite has only been reported for a hydrotalcite with a different Mg/Al ratio under high partial pressure of CO_2 and H_2O [8,16], the mechanism reported by Fricker et al. [30] would match with our mechanism proposed for site C. Formation of potassium carbonate hydrate or potassium magnesium carbonate like reported by Maroño et al. [26] or the formation of dawsonite like reported by Walspurger [31] are also possible candidates. Trying to identify different species after CO_2 adsorption with XRD were unfortunately not possible due to the amorphous structure of the material and the rapid change of the material when exposed to a humid atmosphere. TGA and PBR experiments with different sorbents (potassium promoted alumina and hydrotalcites with a different Mg/Al ratio) will be performed in the near future in order to further investigate the possible chemical species responsible for the different sites reported in this manuscript.

3.3. Validation and accuracy of the model

In this section, the ability of the four site model to quantitatively describe the measured cyclic working capacities during the different experiments is tested. Since all experiments have been conducted at the same base case conditions (T = 400 °C, PCO_2 = 0.66 bar, PH_2O = 0.34 bar, P_{tot} = 1 bar and similar total cycle lengths) constant capacity values for the different sites are expected. We summarized and compared the experimental data with the model predictions for the cyclic mass change for every adsorption/desorption step. The standard deviation between the experimental results and the predicted mass changes by the model was calculated. In order to describe the experimental results with a higher accuracy the cyclic working capacity of the different sites was fitted. The total standard deviation between the experimental results and the model predictions was minimized by adjusting the cyclic working capacity of the different sites proposed within an upper and lower boundary which were inserted in order to ensure that the fitting follows the proposed model. The fitting results for the base case experiment and the given boundaries are summarized in Table 5.

The experimental results of the base case experiment together with the standard deviations between the predictions and experimental results are summarized in the Appendix A (Table A1) for three sets of experiments. Experiments 1–8 were conducted three times to prove the reproducibility of the experiments. In the second set some additional experiments were conducted in order to further prove that the model can predict the cyclic mass change under conditions different from experiments 1–8. In the third set the order of the experiments was revised to validate that indeed

Table 5
Fitted site capacities for the base case experiment in (mg/g).

Model base case					
Site	A	B	C_{eq}	C	D
Boundary low	*0*	*0*	*0*	*0*	*0*
FIT	**8.3**	**11.3**	**5.1**	**11.3**	**5.5**
Boundary high	*13*	*13*	*13*	*13*	*13*

Table 6
Fitting results of the three sets of experiments.

	A	B	C_{eq}	C	D
FITTING RESULTS SET 1	8.06	11.22	5.62	11.73	5.74
FITTING RESULTS SET 2	8.20	10.60	4.54	10.62	6.09
FITTING RESULTS SET 3	8.42	11.52	4.95	10.95	5.26
FITTING RESULTS ALL SETS	8.34	11.28	5.13	11.31	5.53
STD DEVIATION (SET FITTING)	0.14	0.34	0.39	0.41	0.31
VARIANCE (SET FITTING)	0.02	0.15	0.20	0.22	0.12

site D is activated if CO_2 is fed to a hydroxylated sorbent (Experiment 5) and that the starting conditions do not influence the cyclic working capacity of the following steps.

Minimization of the total error always led to the same result for the cyclic working capacities for the different sites, independent on the starting values for the different sites, indicating that indeed a global minimum was found (Table 6). In order to investigate the accuracy of the fitting and the experimental error, the different sites were fitted once for every experimental set separately. The cyclic working capacity determined for the different sites according to Table 5 have been plotted together with the standard deviation if the three different sets were fitted separately. It can be observed that the error between the different experimental sets is quite small. Where for Site A (which is a site which can be independently determined with Experiment 1) the deviation is very small, for the other sites the deviation is somewhat larger. Since the model fitting is based on experimental results, the accuracy of the experiments is mainly responsible for the small discrepancies found for the cyclic working capacities of the different sites.

Details of the measured weight change of the plotted results can be found in Section 3.1 (see Fig. 15) where the mechanism was based on. A table containing all measured weight changes and the deviation of our model to predict the cyclic weight change, can be found in the Appendix A (Table A1). Taking a look at the determined deviation (mg/g) between the model and the experiment, one can notice that the model describes the cyclic mass change very accurately. The highest calculated total standard deviation (average of all standard deviations for one experimental set, Table A1), was calculated being 0.610 mg/g. Inspecting the experimental results it can be seen that the determined standard deviation is in general smaller than the experimental error between two identical experiments (e.g. comparing Experiment 2 of experiment 1 and 2) where a difference in CO_2 cyclic working capacity of 1.18 mg/g was measured. It was already mentioned that the material behavior strongly depends on the conditions as temperature, partial pressure and history of the material. Comparing the measured cyclic mass change of Experiment 2 to Experiment 7, where the same cycle time was used, one can obtain that the mass exchanged is nearly twice as high for Experiment 7 (Table A1). This clearly illustrates how the CO_2 cyclic working capacity can be much improved if H_2O is used instead of N_2 as a balance to CO_2.

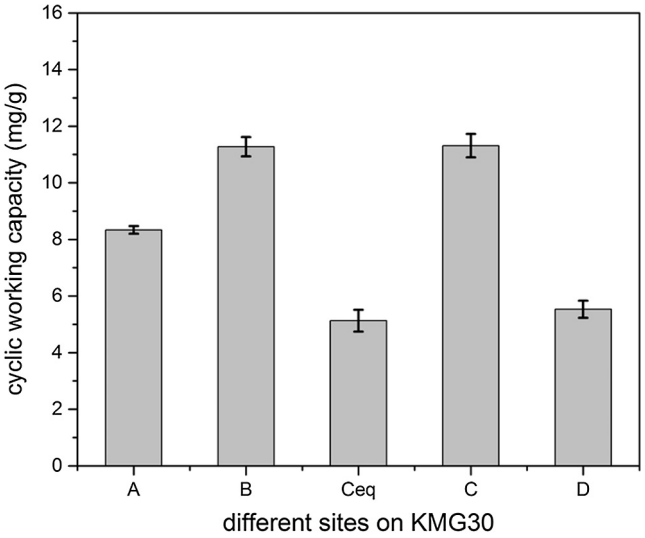

Fig. 15. Site cyclic working capacities determined for KMG30 by minimization of the error between the models and experiments at 400 °C, PCO_2 = 0.66 bar and PH_2O = 0.34 bar (error bars represent the standard deviation between the different sets of experiments).

3.4. Influence of temperature on cyclic working capacity

Analyzing Experiment 1 performed at different temperatures provides information on the temperature dependency of site A for H_2O adsorption. Similarly, Experiment 2 at different temperatures gives the temperature dependency for site B for CO_2 adsorption. These results have been plotted in Fig. 16. It can be discerned that the influence of the operating temperature on the capacity of Site A is opposite to that for Site B, which is in agreement with results reported earlier [27]. From previous studies it is known that the temperature does not affect the adsorption capacity of CO_2, but the desorption kinetics, which can also be obtained from Fig. 16b whereas for Site A clearly the adsorption capacity of Site A is reduced by an increase in operating temperature (Fig. 16a). It can also observed from these figures that the initial H_2O loading of the material is not influenced by temperature, but the total adsorbed amount of H_2O is influenced. On the other hand, for CO_2 the initial CO_2 loading is responsible for the lower cyclic working capacity at lower temperatures due to slower desorption kinetics.

Analyzing the experimental results to determine the cyclic working capacity of site C and D, different approaches were considered since both the capacity of Site C and the capacity of site D cannot be easily determined separately. Based on the proposed model, the cyclic working capacities for the different sites were fitted by using an excel model and the results are plotted in Fig. 17a.

The figure shows that the cyclic working capacities of site A are decreasing and of site B are increasing if the temperature is increased, which has already been described by analyzing the adsorption/desorption kinetics. Site D seems to have a maximum cyclic working capacity at 400 °C. The cyclic mass change seems to increase for C_{eq} (due to Eq. (2)). This increase can be explained with less H_2O being adsorbed at higher temperature and therefore shifting the equilibrium towards the metal carbonate leading to a higher mass change. Interestingly, the total capacity of site C seems to decrease slightly with an increase in temperature indicating that the carbonation of the metal is a slightly exothermic reaction, however, the observed changes are within the experimental error of the experiments and fitting (see the error bars for the experiment at 400 °C). It was already described that Site D is only participating in the adsorption if CO_2 and H_2O are fed together or is active if the material is still wet when exposed to CO_2. Because of this

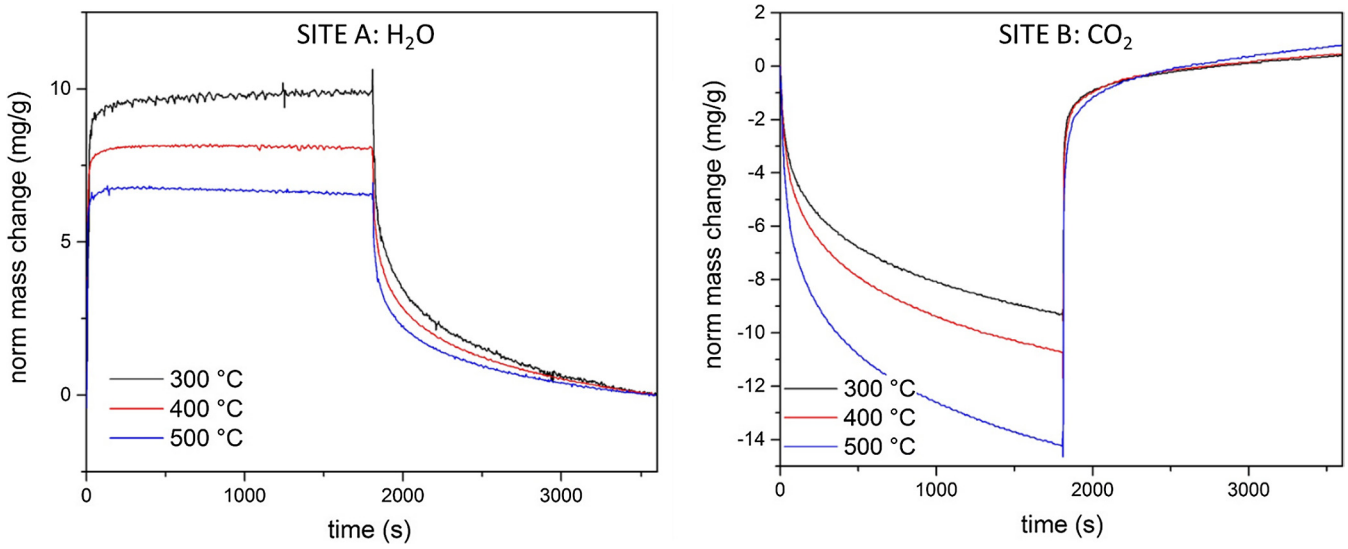

Fig. 16. (a) H_2O dependence on temperature at $P(H_2O) = 0.34$ bar (Site A) (b) CO_2 dependence on the temperature at $P(CO_2) = 0.66$ bar (Site B).

observed behavior it is possible that site D is directly dependent on the capacities of site B and A which represent the weaker and fast adsorption sites, since they can be easily regenerated with N_2.

In order to design a process that can use the cyclic working capacity of the adsorbent very efficiently the total cyclic working capacity of the material is an interesting parameter. Fig. 17b summarizes the cyclic working capacity of CO_2 and H_2O for KMG30 at different operating temperatures. We distinguish between the full CO_2 cyclic working capacity which can be reached if all the sites participate and the cyclic working capacity at equilibrium if CO_2 and H_2O are present together on the material (which is in general the case during WGS reaction). It can be concluded that the sorbent shows the highest CO_2 cyclic working capacity at 400 °C for both conditions (equilibrium or full capacity) which is mainly caused by the higher sorption capacity of CO_2 of site D. This observation based on the four sites model is also confirmed in the literature, where it has already been reported that a hydrotalcite based adsorbent showed a higher CO_2 sorption capacity at 403 °C compared to 306 and 510 °C [10].

4. Conclusions

Smart designed TGA cycles together with experiments in a packed bed reactor were used to develop a mechanism for the interactions between CO_2 and H_2O on a commercial potassium promoted hydrotalcite (KMG30). Four different adsorption sites are necessary to describe the cyclic working capacity for CO_2 and H_2O during different adsorption/desorption cycles with different composition at different temperatures. Two sites A (H_2O) and B (CO_2) can be easily regenerated with N_2. The cyclic working capacity for site B increases at higher temperatures, whereas the cyclic working capacity for site A decreases at higher temperatures. Site D is a site which can be activated if CO_2 and H_2O is present together and its cyclic working capacity depends on the cyclic working capacity of site B and A. The fourth site represents a site which can either adsorb CO_2 or H_2O depending on the feed gas composition. A metal oxide, reacting either to a metal carbonate or a metal hydroxide, was found to be a possible explanation for the observed behavior of the material. With this mechanism the different

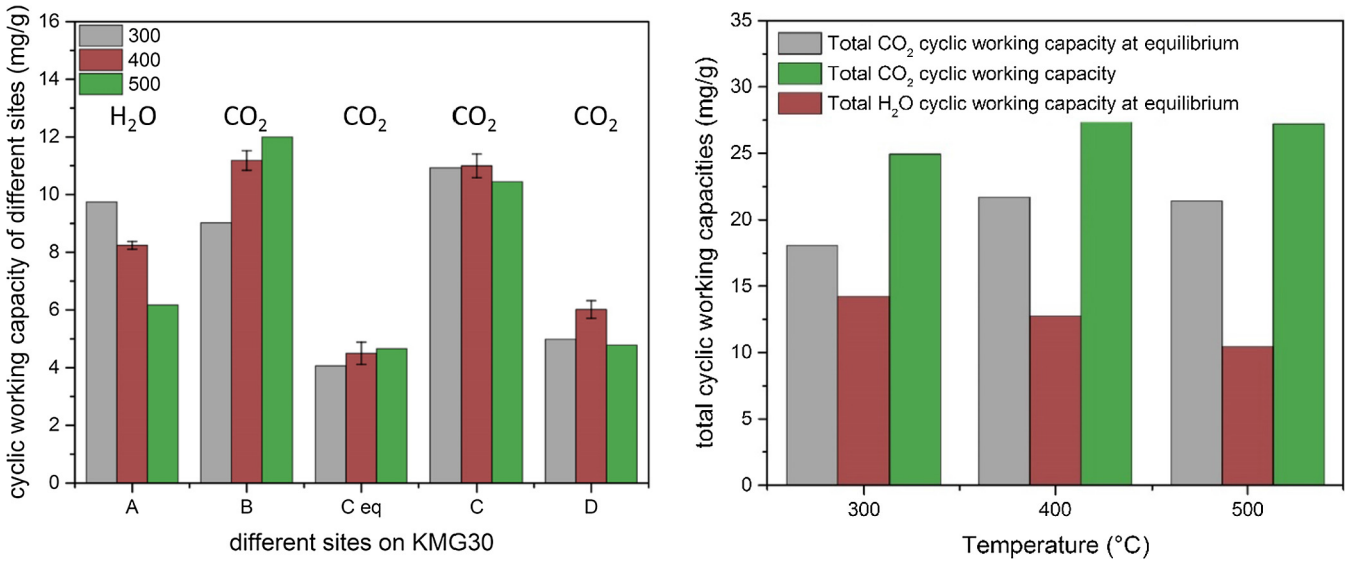

Fig. 17. (a) Cyclic working capacities for the different sites at different temperatures; (b) total CO_2 and H_2O capacities as function of temperature.

measured cyclic working capacity can be explained and we are able to explain the different cyclic working capacity for CO_2 reported in the literature. It is evident from the experiments that H_2O increases the cyclic working capacity of CO_2 significantly. The experimental results have proven that the main reason why steam increases the cyclic working capacity of the adsorbent is due to the regeneration of adsorption sites (site C in particular), which cannot be regenerated with N_2. Regeneration of the adsorbent with H_2O leads to an increase in the CO_2 sorption capacity from 0.3 to 0.72 mmol/g. Feeding H_2O during the adsorption of CO_2 activates more adsorption sites which can increase the cyclic working capacity once more up to 0.85 mmol/g. To the best of our knowledge this is the first time that an explanation is provided for the increased CO_2 cyclic working capacity for a potassium promoted hydrotalcite, as well as a detailed investigation of the different sites involved in the adsorption mechanism. By increasing the CO_2 partial pressure and decreasing the H_2O partial pressure during the adsorption step one can optimize the cyclic working capacity of the adsorbent and thereby increase the efficiency of the process. The proposed cyclic working capacities of the sorbent will significantly decrease in a process for shorter regeneration times, since the desorption is the cyclic working capacity determining step. In order to use the total cyclic working capacity of the adsorbent an optimum between regeneration time can be determined, dependent on the number of columns used in order to design an efficient process. The cyclic working capacity for CO_2 can be increased by 45% if a mixture of H_2O and N_2 is used to regenerate the material due to the activation of more sites using the same cycle time (0.3 compared to 0.53 mmol/g). An operating temperature of 400 °C was found to be best in order to achieve the highest CO_2 cyclic working capacity which is confirmed in the literature. A more detailed kinetic model will be developed in order to describe the transient response of the TGA and simulate the adsorption and desorption of CO_2 and H_2O in a packed bed reactor.

Acknowledgement

The research leading to these results has received support through the ADEM innovation lab program.

Appendix A

The cyclic weight change obtained during the TGA measurements has been summarized in Table A1. In the first column the number of the experiment and in the second column the feed gases are mentioned (according to Table 1, details can be found in Section 2 of the manuscript). In the next five columns we show the cyclic weight change determined by TGA for each step. The deviation of the predicted weight change according to our model compared to the experimental value is shown for each step in grey in the other columns. In the last column, the total average deviation of all experiments performed in one set, where in each step the

Table A1
Summary of experimental results of the base case experiment and standard deviation of proposed model predicting the experimental results.

Base case 400 °C PCO_2 = 0.66 bar PH_2O = 0.34 bar							Model deviation (mg/g)					Total deviation (mg/g)
EXP	Experimental cycle description	CO2	CO_2/H_2O	N_2	N_2/H_2O	N_2	CO_2	CO_2/H_2O	N_2	N_2/H_2O	N_2	
1	$H_2O/N_2 \Rightarrow N_2$				7.90	−8.06				0.26	0.15	0.447
2	$CO_2 \Rightarrow N_2$	11.57		−10.71			0.60		0.00			
3	$CO_2 \Rightarrow N_2 \Rightarrow N_2/H_2O \Rightarrow N_2$	22.96		−12.30	−2.12	−7.85	0.35		1.12	0.96	0.30	
4	$CO_2/H_2O \Rightarrow CO_2 \Rightarrow N_2 \Rightarrow N_2/H_2O \Rightarrow N_2$	−1.95	33.72	−15.17	−6.48	−8.51	0.09	1.94	0.52	0.20	0.17	
5	$CO_2 \Rightarrow CO_2/H_2O \Rightarrow N_2 \Rightarrow N_2/H_2O \Rightarrow N_2$	24.94	7.69	−19.27	−4.20	−8.32	1.04	0.12	0.51	1.04	0.03	
6	$CO_2/H_2O \Rightarrow N_2 \Rightarrow N_2/H_2O \Rightarrow N_2$		31.34	−18.91	−3.72	−8.20		0.25	0.76	0.71	0.05	
7	$CO_2/H_2O \Rightarrow N_2/H_2O$		21.71		−21.29			0.00		0.29		
8	$CO_2/H_2O \Rightarrow N_2/H_2O \Rightarrow N_2$		30.27		−21.23	−8.35		0.21		0.34	0.06	
Additional experiment 400 °C PCO_2 = 0.66 bar PH_2O = 0.34 bar							Model deviation (mg/g)					Total deviation (mg/g)
No	Experimental cycle description	CO_2	CO_2/H_2O	N_2	N_2/H_2O	N_2	CO_2	CO_2/H_2O	N_2	N_2/H_2O	N_2	
1	$H_2O/N_2 \Rightarrow N_2$				8.05	−8.20				0.16	0.05	0.544
2	$CO_2 \Rightarrow N_2$	10.39		−9.49			0.23		0.87			
3	$CO_2 \Rightarrow N_2 \Rightarrow N_2/H_2O \Rightarrow N_2$	20.66		−11.28	−1.28	−7.61	1.28		0.40	1.56	0.47	
4	$CO_2/H_2O \Rightarrow CO_2 \Rightarrow N_2 \Rightarrow N_2/H_2O \Rightarrow N_2$	−2.11	32.62	−15.37	−5.01	−8.87	0.03	1.16	0.66	0.85	0.42	
5	$CO_2 \Rightarrow CO_2/H_2O \Rightarrow N_2 \Rightarrow N_2/H_2O \Rightarrow N_2$	24.01	7.48	−19.03	−3.51	−8.47	0.38	0.02	0.68	0.56	0.14	
6	$CO_2/H_2O \Rightarrow N_2 \Rightarrow N_2/H_2O \Rightarrow N_2$		30.43	−18.78	−3.22	−7.95		0.39	0.85	0.35	0.22	
7	$CO_2/H_2O \Rightarrow N_2/H_2O$		21.30		−20.78			0.29		0.66		
8	$CO_2/H_2O \Rightarrow N_2/H_2O \Rightarrow N2$		29.14		−20.77	−8.24		0.59		0.66	0.02	
9	$N_2/H_2O \Rightarrow CO_2 \Rightarrow N_2$	16.78		−13.72	−3.11		0.35		0.65	0.27		
10	$CO_2/H_2O \Rightarrow CO_2 \Rightarrow N_2/H_2O$	−2.15	21.49		−19.01		0.06	0.86		1.15		
11	$CO_2/H_2O \Rightarrow N_2/H_2O \Rightarrow CO_2$	16.03	5.16		−20.95		0.18	0.89		1.24		
Reversed order 400 °C PCO_2 = 0.66 bar PH_2O = 0.34 bar							Model deviation (mg/g)					Total deviation (mg/g)
No	Experimental cycle description	CO_2	CO_2/H_2O	N_2	N_2/H_2O	N_2	CO_2	CO_2/H_2O	N_2	N_2/H_2O	N_2	
4	$CO_2/H_2O \Rightarrow CO_2 \Rightarrow N_2 \Rightarrow N_2/H_2O \Rightarrow N_2$	−2.40	34.13	−16.44	−5.18	−8.72	0.23	2.23	1.42	0.73	0.32	0.610
5	$CO_2 \Rightarrow CO_2/H_2O \Rightarrow N_2 \Rightarrow N_2/H_2O \Rightarrow N_2$	25.12	7.82	−20.00	−3.26	−9.14	1.17	0.22	0.01	0.38	0.62	
1	$H_2O/N_2 \Rightarrow N_2$				7.64	−9.09				0.44	0.58	
2	$CO_2 \Rightarrow N_2$	12.88		−12.44			1.53		1.22			
3	$CO_2 \Rightarrow \Rightarrow N_2 \Rightarrow N_2/H_2O \Rightarrow N_2$	24.44		−13.47	−2.56	−8.27	0.68		1.24	0.65	0.00	
6	$CO_2/H_2O \Rightarrow N_2 \Rightarrow N_2/H_2O \Rightarrow N_2$		31.10	−18.58	−3.24	−8.37		0.08	0.99	0.36	0.07	
7	$CO_2/H_2O \Rightarrow N_2/H_2O$		21.43		−20.85			0.90		1.31		
8	$CO_2/H_2O \Rightarrow N_2/H_2O \Rightarrow N_2$		29.87		−20.97	−8.62		0.79		1.23	0.25	
12	$CO_2 \Rightarrow H_2O$	16.34			−16.68		0.04			0.28		
1	$N_2 \Rightarrow H_2O/N_2$				8.27	−8.38				0.00	0.08	
12	$CO_2 \Rightarrow H_2O$	16.16			−16.28		0.09			0.00		

experimental results obtained by TGA were compared with the predicted weight change of our model.

References

[1] UNFCCC, Report of the Conference of the Parties on its twenty-first session, held in Paris from 30 November to 13 December 2015, Unfccc, vol. 01192, no. February, 2015.

[2] F. Birol, Redrawing the Energy-Climate MAP: World Energy Outlook Special Report World Energy Outlook Special Report Paris, 2013, p. 134.

[3] M. Gazzani, E. MacChi, G. Manzolini, CO_2 capture in integrated gasification combined cycle with SEWGS – Part A: thermodynamic performances, Fuel 105 (2013) 206–219.

[4] J. Boon, V. Spallina, Y. van Delft, M. van Sint Annaland, Comparison of the efficiency of carbon dioxide capture by sorption-enhanced water–gas shift and palladium-based membranes for power and hydrogen production, Int. J. Greenhouse Gas Control 50 (2016) 121–134.

[5] G. Manzolini, E. MacChi, M. Gazzani, CO_2 capture in integrated gasification combined cycle with SEWGS – Part B: economic assessment, Fuel 105 (2013) 220–227.

[6] E.R. van Selow, P.D. Cobden, H.A.J. van Dijk, S. Walspurger, P.A. Verbraeken, D. Jansen, Qualification of the ALKASORB sorbent for the sorption-enhanced water-gas shift process, Energy Proc. 37 (2013) 180–189.

[7] A.D. Ebner, S.P. Reynolds, J.A. Ritter, Understanding the adsorption and desorption behavior of CO_2 on a K-promoted hydrotalcite-like compound (HTlc) through nonequilibrium dynamic isotherms, Ind. Eng. Chem. Res. 50 (2006) 6387–6392.

[8] S. Walspurger, P.D. Cobden, O.V. Safonova, Y. Wu, E.J. Anthony, High CO(2) storage capacity in alkali-promoted hydrotalcite-based material: in situ detection of reversible formation of magnesium carbonate, Chemistry 16 (42) (2010) 12694–12700.

[9] K.B. Lee, A. Verdooren, H.S. Caram, S. Sircar, Chemisorption of carbon dioxide on potassium-carbonate-promoted hydrotalcite, J. Colloid Interface Sci. 308 (1) (2007) 30–39.

[10] E.L.G. Oliveira, C.A. Grande, A.E. Rodrigues, CO_2 sorption on hydrotalcite and alkali-modified (K and Cs) hydrotalcites at high temperatures, Sep. Purif. Technol. 62 (2008) 137–147.

[11] D.P. Debecker, E.M. Gaigneaux, G. Busca, Exploring, tuning, and exploiting the basicity of hydrotalcites for applications in heterogeneous catalysis, Chemistry 15 (16) (2009) 3920–3935.

[12] W.T. Reichle, Catalytic reactions by thermally activated, synthetic, anionic clay minerals, J. Catal. 557 (1985) 547–557.

[13] F. Cavani, F. Trifiro, A. Vaccari, Hydrotalcite-type anionic clays: preparation, properties and applications, Catal. Today 11 (1991) 173–301.

[14] N.N.A.H. Meis, J.H. Bitter, K.P. De Jong, On the influence and role of alkali metals on supported and unsupported activated hydrotalcites for CO_2 sorption, Ind. Eng. Chem. Res. (2010) 8086–8093.

[15] S. Walspurger, L. Boels, P.D. Cobden, G.D. Elzinga, W.G. Haije, R.W. van den Brink, The crucial role of the K+-aluminium oxide interaction in K+-promoted alumina- and hydrotalcite-based materials for CO_2 sorption at high temperatures, ChemSusChem 1 (7) (2008) 643–650.

[16] E.R. Van Selow, P.D. Cobden, A.D. Wright, R.W. Van Den Brink, D. Jansen, Improved sorbent for the sorption-enhanced water-gas shift process, Energy Proc. 4 (2011) 1090–1095.

[17] W. Reichle, S. Kang, D. Everhardt, The nature of the thermal decomposition of a catalytically active anionic clay mineral, J. Catal. 7 (1986) 352–359.

[18] D. Tichit, C. Gérardin, R. Durand, B. Coq, Layered double hydroxides: precursors for multifunctional catalysts, Top. Catal. 39 (1–2) (2006) 89–96.

[19] E.R. Van Selow, P.D. Cobden, P.A. Verbraeken, J.R. Hufton, R.W. Van Den Brink, Carbon capture by sorption-enhanced water-gas shift reaction process using hydrotalcite-based material, Ind. Eng. Chem. Res. (2009) 4184–4193.

[20] P.D. Cobden, P. van Beurden, H.T.J. Reijers, G.D. Elzinga, S.C.A. Kluiters, J.W. Dijkstra, D. Jansen, R.W. van den Brink, Sorption-enhanced hydrogen production for pre-combustion CO_2 capture: thermodynamic analysis and experimental results, Int. J. Greenhouse Gas Control 1 (2) (2007) 170–179.

[21] J. Boon, P.D. Cobden, H.A.J. van Dijk, M. van Sint Annaland, High-temperature pressure swing adsorption cycle design for sorption-enhanced water–gas shift, Chem. Eng. Sci. 122 (2015) 219–231.

[22] E. van Dijk, S. Walspurger, P. Cobden, R. van den Brink, Testing of hydrotalcite based sorbents for CO_2 and H_2S capture for use in sorption enhanced water gas shift, Energy Proc. 4 (2011) 1110–1117.

[23] M.H. Halabi, M.H.J.M. de Croon, J. van der Schaaf, P.D. Cobden, J.C. Schouten, High capacity potassium-promoted hydrotalcite for CO_2 capture in H_2 production, Int. J. Hydrogen Energy 37 (5) (2012) 4516–4525.

[24] J. Boon, P.D. Cobden, H.A.J. van Dijk, C. Hoogland, E.R. van Selow, M. van Sint Annaland, Isotherm model for high-temperature, high-pressure adsorption of CO_2 and H_2O on K-promoted hydrotalcite, Chem. Eng. J. 248 (2014) 406–414.

[25] H.T.J. Reijers, S.E.A. Valster-Schiermeier, P.D. Cobden, R.W. Van Den Brink, Hydrotalcite as CO_2 sorbent for sorption-enhanced steam reforming of methane, Ind. Eng. Chem. Res. 45 (2006) 2522–2530.

[26] M. Maroño, Y. Torreiro, L. Gutierrez, Influence of steam partial pressures in the CO_2 capture capacity of K-doped hydrotalcite-based sorbents for their application to SEWGS processes, Int. J. Greenhouse Gas Control 14 (2013) 183–192.

[27] K. Coenen, F. Gallucci, P. Cobden, E. van Dijk, E. Hensen, M. van, S. Annaland, Chemisorption working capacity and kinetics of CO_2 and H_2O of hydrotalcite-based adsorbents for sorption-enhanced water-gas-shift applications, Chem. Eng. J. 293 (2016) 9–23.

[28] E. van Dijk, S. Walspurger, P.D. Cobden, R.W. van den Brink, F.G. de Vos, Testing of hydrotalcite-based sorbents for CO_2 and H_2S capture for use in sorption enhanced water gas shift, Int. J. Greenhouse Gas Control 5 (2011) 505–511.

[29] J.R. Hufton, S. Mayorga, S. Sircar, Sorption-enhanced reaction process for hydrogen production, AIChE J. 45 (2) (1999) 248–256.

[30] K.J. Fricker, A.H.A. Park, Effect of H_2O on $Mg(OH)_2$ carbonation pathways for combined CO_2 capture and storage, Chem. Eng. Sci. 100 (2013) 332–341 (no. March 2016).

[31] S. Walspurger, P.D. Cobden, W.G. Haije, R. Westerwaal, G.D. Elzinga, O.V. Safonova, In situ XRD detection of reversible dawsonite formation on alkali promoted alumina: a cheap sorbent for CO_2 capture, Eur. J. Inorg. Chem. 2010 (17) (2010) 2461–2464.

[32] M. Maroño, Y. Torreiro, L. Montenegro, J. Sánchez, Lab-scale tests of different materials for the selection of suitable sorbents for CO_2 capture with H_2 production in IGCC processes, Fuel 116 (2014) 861–870.